Continental break-up history of a deep magma-poor margin based on seismic reflection data (northeastern Gulf of Aden margin, offshore Oman)

Julia Autin, Sylvie Leroy, Marie-Odile Beslier, Elia D'Acremont, Philippe Razin, Alessandra Ribodetti, Nicolas Bellahsen, Cécile Robin, Khalfan Al Toubi

Continental break-up history of a deep magma-poor margin based on seismic reflection data (north-eastern Gulf of Aden margin, offshore Oman)

Julia Autin[1], Sylvie Leroy[1, 2], Marie-Odile Beslier[3], Elia d'Acremont[1], Philippe Razin[4], Alessandra Ribodetti[3], Nicolas Bellahsen[1], Cécile Robin[5] and Khalfan Al Toubi[6]

[1] UMR 7193, ISTeP, UPMC Univ Paris 6, Case 129, 4 place Jussieu, 75252 Paris Cedex 05, France
[2] UMR 7193, ISTeP, CNRS, Case 129, 4 place Jussieu, 75252 Paris Cedex 05, France
[3] CNRS-Géosciences Azur-UMR 6526, OOV, B.P. 48, 06235 Villefranche-sur-Mer cedex, France
[4] EGID, Université Bordeaux 3, 33607 Pessac cedex, France
[5] Geosciences Rennes, Université de Rennes 1, Campus de Beaulieu, 35042 Rennes Cedex, France
[6] Sultan Qaboos University, Earthquake Monitoring centre, Al Khod PC 123, Sultanate of Oman

Corresponding author: Julia Autin, julia.autin@gmail.com

Abbreviated title: *Continental break-up history of the north-eastern Gulf of Aden*

SUMMARY

Rifting between Arabia and Somalia started around 35 Ma ago followed by spreading at 17.6 Ma in the eastern part of the Gulf of Aden. The first-order segment between the Alula-Fartak and Socotra-Hadbeen fracture zones is divided into three second-order segments with different structure and morphology. Seismic reflection data were collected during the Encens Cruise in 2006 on the north-eastern margin [?of the Gulf of Aden]. In this study, we present the results of Pre-Stack Depth Migration (PSDM) of the multichannel seismic data from the western segment of the margin, which allows us to propose a tectono-stratigraphic model of the evolution of this segment from rifting to the present day. The chronological interpretation of the sedimentary sequences is mapped out in relation to the onshore observations and existing dating. After a major development of syn-rift grabens and horsts, the deformation became localised into zones with thinner crust. This deformation occurred within the distal margin graben (DIM) at the northern boundary of the Ocean–Continent Transition (OCT), represented by the OCT ridge. During the early stages of formation of the OCT, differential uplift induced a submarine landslide on top of the deepest tilted block, and crustal deformation was restricted to the southern part of the DIM

1

graben, where the continental break-up finally occurred. Initial seafloor spreading was followed by post-rift magmatic events (flows, sills and volcano-sedimentary wedge), whose timing is constrained by an analysis of the sedimentary cover of the OCT ridge, correlated with onshore stratigraphy. The OCT ridge may represent exhumed serpentinized mantle intruded by post-rift magmatic material, which modified the OCT after its emplacement.

Keywords: continental margins, ocean-continent transition, rifting, vertical movements, multichannel seismic reflection, Gulf of Aden.

1 INTRODUCTION

At present, an evolution is taking place in conceptual ideas concerning the sedimentary architecture and tectonic evolution of rifted margins. Although we can observe different phases of subsidence, uplift and volcanism, as well as different conditions of break-up of the continental crust, these differences are not well explained by classical models of rifted margin formation (McKenzie 1978; Wernicke 1985). Early models were based implicitly on the assumption that seafloor spreading directly follows rifting and that continental break-up is well defined in time and space in the sedimentary record in the form of tectonic structures, subsidence and unconformities. These ideas are now being challenged by new observations, and the most recent numerical and conceptual models suggest that continental break-up develops in a complex way involving different processes of extension operating simultaneously in different parts of the margin (Lavier & Manatschal 2006; Nagel & Buck 2007; Reston & Pérez-Gussinyé 2007; Weinberg et al. 2007; Huismans & Beaumont 2008). New insights from the north-eastern margin of the Gulf of Aden allow us to propose just such a complex evolution.

The Gulf of Aden is a young oceanic basin. While volcanic margins are observed in the western part of the Gulf in relation to the Afar hotspot (Tard *et al.* 1991), the eastern Gulf

exhibits magma-poor margins (d'Acremont *et al.* 2005). The superficial structure of the eastern conjugate margins has been studied recently using a geophysical dataset (bathymetry, seismic reflection, gravity and magnetic data) that reveals first and second-order segmentation (d'Acremont *et al.* 2005; d'Acremont *et al.* 2006). Nevertheless, the deep structure of the margins was poorly imaged and not well understood. The data used in this study are taken from the Encens cruise carried out in February/March 2006 on board R-V L'Atalante (Leroy *et al.* 2006). The cruise was conducted in the north-eastern Gulf of Aden continental margin (Fig. 1), with acquisition of multibeam bathymetry, 360-channel seismic reflection (10 km spaced profiles), gravity and magnetic data.

In this work, we focus our study on the Ashawq-Salalah segment (Fig. 2) of the Encens cruise area (Leroy *et al.* 2006; Leroy *et al.* submitted), corresponding to the westernmost third of the first-order segment between the Alula-Fartak (AFFZ) and Socotra-Hadbeen fracture zones (SHFZ, Fig. 1). The segmented margin contains large lateral variations in terms of crustal structure, sedimentation and morphology. Notably, the Ocean–Continent Transition (OCT) displays different morphological features along the north-eastern Gulf of Aden margin (Leroy *et al.* submitted). Therefore, the evolution of each second-order segment may vary. Separate studies of these segments can thus contribute to our understanding of the development of the whole margin. We pay particular attention to the structural and sedimentary architecture of the deep margin, while integrating offshore features with onland sedimentological observations. We focus on the multichannel seismic profiles (MCS) of the western part of the survey, concentrating in particular on one across-margin profile (ENC34), which strikes parallel to the direction of extension (N026°E). This ENC34 line was processed by the Pre-Stack Depth Migration (PSDM) method.

We propose a scenario for the evolution of the margin and the OCT, including the onshore-offshore link. Although the nature of the OCT is not definitively known and requires further interpretation of wide-angle seismic results, we can nevertheless propose a hypotheses on the

break-up history of this margin segment. The post-rift cover contains several unconformities which we interpret as reflecting magmatic events and vertical movements during post-rift times.

2 TECTONOSEDIMENTARY EVOLUTION OF THE STUDIED AREA

2.1 Kinematic context and structural evolution

The Gulf of Aden is an oceanic basin separating Arabia from Somalia (Fig. 1). The inception [or earliest occurrence] of the Afar hotspot is recorded at 45 Ma (George *et al.* 1998), with a peak activity at ca. 30 Ma (Hofmann *et al.* 1997; Ebinger & Sleep 1998; Kenea *et al.* 2001). During the Late Eocene, the western part of the Gulf was uplifted due to activity of the Afar hotspot and the Gulf of Aden began to open. The rifting started 35 Ma ago all along the [?axis of the] Gulf (Roger *et al.* 1989; Bott *et al.* 1992; Watchorn *et al.* 1998), followed by oceanic spreading from 17.6 Ma in the eastern part of the Gulf (Leroy *et al*. 2004) and around 20 Ma near the Owen fracture zone (Fournier *et al.* 2008). The orientation of the Gulf (N75°E) and the kinematics of opening (ca. N30°E-trending divergence) indicate oblique rifting (Fantozzi & Sgavetti 1998; Lepvrier *et al.* 2002; Huchon & Khanbari 2003; Fournier *et al.* 2004; Bellahsen *et al.* 2006). The Euler pole of opening is currently at 24.01°N, 24.57°E (Fournier *et al.* 2001), so that the spreading rate increases from 13 mm/yr (parallel to N035°E) in the west, to 18 mm/yr in the east (parallel to N025°E) (Jestin *et al.* 1994; Vigny *et al.* 2006) (Fig. 1). Two major discontinuities divide the Gulf of Aden into three parts (Manighetti *et al.* 1997): (1) The Shukra-El Sheik fracture zone separates the central part from the westernmost part, which is strongly affected by volcanism related to the Afar hotspot (Fig. 1) (Manighetti *et al.* 1998; Dauteuil *et al.* 2001; Hébert *et al.* 2001). (2) The AFFZ separates the central Gulf from the eastern Gulf (Tamsett & Searle 1990).

2.2 Onshore sedimentation on the north-eastern margin

The onshore part of the study area is located in the Dhofar region (Sultanate of Oman). The crystalline basement cropping out in the Mirbat peninsula (Fig. 2) comprises gneisses (ca. 1000–810 Ma, source rocks > 1300 Ma), calc-alkaline igneous suites (830–780 Ma), aplites and pegmatites (770–750 Ma) and granodiorites (ca. 750–700 Ma) (Mercolli *et al.* 2006). The basement most probably extends further westward under the Ashawq-Salalah basin, although its evolution may differ slightly along the margin due to a different exhumation history. The Mesozoic pre-rift units record a transgression during the Barremian-Aptian (Platel & Roger 1989). The Tertiary pre-rift succession, known as the Hadhramaut group (Fig. 3), contains two thick shallow-marine shelf units: the Umm Er Radhuma Formation (Paleocene to Lower Eocene) and the Dammam Formation (Lower Lutetian to Bartonian). A period of successive emergence (evaporites and dolomites associated with mud-cracks from the Rus Formation, 60 m thick) separates the two shelves (Fig. 3). During the Eocene, a broad uplift of the Arabian plate is recorded by regression on all the margins. Nevertheless, the accumulation of sediments (ca. 100 m) during the Priabonian requires local subsidence at the future location of the north-eastern margin (Aydim Formation, lacustrine and palustrine environments, Roger *et al.* 1989). The Aydim Formation is unconformably overlain by the syn-rift units (Platel & Roger 1989).

The syn-rift succession is described as sediments localised in strongly subsiding grabens showing a regional transgression linked to the rifting subsidence (Fig. 3) (Platel *et al.* 1992). The Priabonian to early Oligocene Zalumah Formation comprises sabkhas and dolomitic paleosols located in certain small areas (Roger *et al.* 1989). Shallow-marine and shoreline sediments make up the Ashawq Formation (Rupelian to basal Chattian), the base of which is composed of clay and sand belonging to the Shizar member. At the end of the early Oligocene, the rifting intensified and became focused on major listric faults leading to the

deposition of the base of the Mughsayl Formation during a transgressive episode (Roger *et al.* 1989). This episode is characterized by turbiditic sedimentation at the foot of the slopes and rapid accumulation of prograding sedimentary prisms.

The top of the Mughsayl Formation is dated as early Miocene (Middle Burdigalian) (Roger *et al.* 1989). The upper Mughsayl Formation shows a sequence of regressive facies overlain by a Gilbert-delta succession indicative of a regression induced by general uplift of the margin (Fig. 3, Leroy *et al.* 2007). The Gilbert delta marks a rapid emergence of the margin and the infilling of its proximal part.

The post-rift sequence is identified by signs of emergence and continental deposits. It lies unconformably on top of the syn-rift sediments, following a phase of emergence during which there is no sedimentary record onshore (Fig. 3). The Adawnib Formation (Langhian to Serravallian) is characterized by a shallow-marine environment during a transgressive trend. Regression began at the beginning of the late Miocene (Fig. 3) (Platel *et al.* 1992). The Nar Formation, which is Late Miocene-Pliocene in age, contains continental detrital material. The conglomeratic deposits of the Nar Formation provide evidence of to the final emergence of the Dhofar. The preservation of a thick section of conglomerates (around 30 m) indicates subsidence of the margin.

2.3 Previous studies in the offshore domain

Previous studies of the eastern Gulf of Aden conjugate margins were undertaken during the Encens-Sheba cruise of June/July 2000 aboard R/V Marion Dufresne between the AFFZ and SHFZ (Fig. 1). Multibeam bathymetry, three-channel seismic reflection (40-km spaced profiles), gravity and magnetics data were gathered to compare the structure of the conjugate margins and reconstruct their evolution (Leroy *et al.* 2004; d'Acremont *et al.* 2005; d'Acremont *et al.* 2006). East of the AFFZ, the conjugate margins are 200 km apart and located about 850 km east of the Afar hotspot. They are considered to be non-volcanic

because the data do not show any evidence of syn-rift volcanism in the study area: seismic surveys have failed to reveal any SDRs or flat and highly reflective volcanic flow units in the OCT or on the margins (d'Acremont *et al.* 2005; d'Acremont *et al.* 2006). Moreover, the onland stratigraphy of the upper margins does not comprise any syn-rift volcanic suites. This suggests that the surface expression of the plume does not extend eastward of the AFFZ.

Between the two major first-order AFFZ and SHFZ transform faults, a second-order segmentation is observed offshore, separating the conjugate margins into three N110°E-trending segments (Fig. 2) (d'Acremont *et al.* 2005). Transfer faults corresponding to the second-order segmentation have not been observed on the proximal part of the margin.

d'Acremont *et al.* (2005) show that the margins are asymmetric: offshore, the northern margin is narrower and steeper (125-180 km) than the southern margin (300 km). These authors (op. cit.) relate this asymmetry to inherited Jurassic/Cretaceous rifts, suggesting that the two syn-rift phases distinguished on the seismic profiles are associated with successive uplifts of the rift shoulders. Elsewhere, the syn-rift series are often thinner, rarely displaying fan-like sedimentary wedges. Two offshore post-rift units make up a complete regressive cycle (post-rift 1) and a transgressive cycle (post-rift 2), corresponding to uplift and subsidence episodes following the break-up, respectively.

The combined analysis of seismic reflection data as well as free-air gravity and magnetic anomalies reveals a narrow (20–30 km) transitional zone on both margins between the oceanic and the continental domains (OCT), characterised by the following features (d'Acremont *et al.* 2005): (1) The acoustic basement is clearly faulted and generally concealed beneath the sediment cover. (2) The occurrence of sediments, observed in the OCT area and not observed on the oceanic crust, considered as contemporaneous with the deformation of the OCT basement. The authors called these deposits 'syn-OCT sediments'. They are covered by post-rift deposits. (3) A negative gradient of the free-air gravity anomaly from oceanic to continental domains is due to an edge effect generated by the juxtaposition of these two types

of crust (Worzel 1968). (4) The magnetics data are generally quiet and flat in the OCT, but locally display high-amplitude anomalies. The amplitudes are low for an oceanic crust but high for a continental crust.

The authors propose several possible compositions for the OCT. (1) The OCT could be made up of ultra-stretched continental crust intruded by magmatic bodies. Indeed, gravity models constrained from magnetics and seismic reflection data indicate highly thinned crust. Moreover, non-oceanic high-amplitude magnetic anomalies are observed where there are no syn-rift sediments (d'Acremont *et al.* 2005). (2) Locally, the nature of the OCT could either correspond to an area of ultra-slow spreading oceanic crust or exhumed serpentinized mantle (d'Acremont *et al.* 2006).

Magnetic anomaly 5d (17.6 Ma) represents the earliest evidence for oceanic spreading in the study area (Leroy *et al.* 2004). The early oceanic segmentation appears to be directly related to the continental margin segmentation. Subsequent magmatic activity and regional kinematic changes strongly control the development of segmentation (d'Acremont *et al.* 2006; d'Acremont *et al.* submitted).

3 DATA COLLECTION AND PROCESSING

3.1 Data acquisition

We use the integrated navigation system of the Ifremer/Genavir shipboard equipment, which records 360 channels at a sampling rate of 4 ms. The seismic source used in the study area allows good sediment resolution and deep reflector imaging. A tuned array of 14 air guns (first pulse synchronised) totalling 42.5 l (2,594 in^3) was shot at 50 m intervals (at about 20 s intervals). The receiver array consisted of 360 groups of hydrophones spaced at 12.5 m intervals for a total array length of 4,500 m. It comprises 30 active sections, each 150 m in

length. The geometry of the shots and receivers were set according to GPS navigation data. This survey had a nominal 45-fold coverage.

3.2 Conventional processing

All lines underwent a careful processing strategy developed in collaboration with the Geosciences Azur Laboratory (Sage *et al.* 2006). Additionally, a preserved-amplitude treatment step was adapted for pre-processing of the ENC34 line (Fig. 4) before the pre-stack depth migration.

The processing sequence (Geocluster® 3100 and 4100, Linux Red Hat) included external mute dynamic velocity corrections determined by three successive velocity analyses, gain reinforcement, spherical divergence correction, spiking deconvolution, Radon (τ, p) domain and controlled frequency-wave number (F, k) domain antimultiples, internal mute of near offsets, stack, constant-velocity Kirchhoff migration, (F, k) domain filtering, (x, t) domain filtering and dynamic amplitude equalization. The band-pass filtering was between 5 and 125 Hz and varied according to the line features. The ENC32, ENC34 and ENC35 lines (Figs 5 and 6) were processed with this method.

3.3 Pre-stack depth migration method

We applied preserved amplitude pre-stack depth migration (PSDM) (Thierry *et al.* 1999; Operto *et al.* 2003) on the ENC34 line (Fig. 4) to obtain images of the deep and shallow reflectors. The PSDM was performed in the Geosciences Azur Laboratory. A preserved amplitude pre-processing was applied to the ENC34 line before the PSDM. An initial velocity macro-model was estimated from velocity analyses. To improve the migrated image at depths greater than 6 km, the PSDM processing integrates - ?at the depth of interest - the preliminary velocity model of a concordant wide-angle seismic profile (ENCR02 on Fig. 2, Watremez *et al.* 2009) following the method proposed by Agudelo (2005). The velocity model was

9

constructed with the reflection model down to 5 km, and with the wide-angle model from 8 to 20 km. The velocity models are combined between 5 and 8 km. Inaccuracy in the initial velocity macro-model can dramatically affect the results. If the velocity macro-model is incorrect, the reflectors are mislocated at depth and their amplitude can be under- or over-estimated. Thus, we corrected the velocity macro-model by the classical approach called 'migration-velocity-analysis'. This simple and efficient method proposed by Al-Yahya (1987) was implemented during the PhD thesis of Agudelo (2005). The local correction function for the velocity macro-model was estimated from Iso-X and semblance panels (Al-Yahya 1987). An iterative correction of the macro-model was performed to obtain flat reflectors in Iso-X panels and semblance panels centred around 1 (Al-Yahya 1987). When these ?mandatory/necessary conditions were satisfied, the Iso-X panels were stacked to produce an accurate final migrated image.

4 SEISMIC STRATIGRAPHY OF THE ASHAWQ-SALALAH MARGIN SEGMENT

All across-margin lines of the Encens cruise in the Ashawq-Salalah segment (Fig. 2) reveal similar general morphologies (Figs 5 and 6): on the proximal margin, we observe a shallow horst delimiting a deep so-called 'perched graben'. In the deep margin, sediments smooth out the basement topography, which is marked by a basement high. This basement high, although generally buried, separates a deep graben at the foot of the continental slope (called the distal margin graben, or DIM graben) from the oceanic basin.

Our study confirms the continuity of the basement highs and the adjacent grabens all along the Ashawq-Salalah segment (d'Acremont *et al.* 2005). However, the new bathymetry and basement maps give evidence of some changes in the trend and morphology of the structural features along strike (Figs 5 and 6). The deepest basement high, located in the OCT domain

and here called the OCT ridge, is overlain by a broad bathymetric high of low amplitude. Its trend changes from WNW–ESE to the west of the ENC34 line to E–W on its eastern side (Figs 5a and b). As the major fault scarp marking the continental slope has a constant E–W strike, the change in the OCT ridge trend is concomitant with an eastward widening of the DIM graben (from 20 to 27 km). On the proximal margin, the basement high is progressively buried eastward of the ENC34 line (black arrow on Fig. 6), where it appears much wider than on the adjacent lines. The perched graben is generally narrow (16 to 19 km), and particularly so on the ENC34 line where it is only 10 km wide. South of the OCT ridge, the oceanic basin opens toward the deep oceanic floor.

Although our results do not significantly change the limits of the three crustal domains previously located by d'Acremont *et al.* (2005; 2006), they suggest a change in the limit between the continental domain and the OCT. According to the interpretation of the new MCS lines, we shift this limit southward from the mid part to the southern boundary of the DIM graben (see below).

 To be consistent throughout the study area, the following seismostratigraphic facies descriptions are based on the time-migrated seismic lines and not on the depth migrated profile. Figure 3 summarizes the seismic units observed in the area and their correlation with the onshore formations. On rifted margins, the deep distal sedimentation is generally of mainly detrital nature and occurs after the proximal parts have been eroded. Thus, offshore sedimentation may be thick when onshore sedimentation is poorly developed or missing. Likewise, when onshore sedimentation is thick, offshore sedimentation may be poor (moderately thin deposits on Fig. 3). Without well data, correlations between onshore and offshore series are partly based on these principles and on the geometries of the sediments. Indeed, syn-tectonic sedimentary wedges observed on the proximal margin may be older than or coeval with the sedimentary wedges on the distal margin.

4.1 Acoustic basement

The top of the acoustic basement (Fig. 6, thick line) corresponds to a strong reflector between an upper well layered sedimentary seismic facies and a lower more chaotic facies. It is generally well imaged on the MCS lines. However, further interpretation of the PSDM line shows that it does not fit any single stratigraphic boundary on the margin. It generally corresponds to the top of the pre-rift series in the deep perched basin, or the top of the syn-tectonic series interpreted as the syn-rift sediments in the DIM graben. In these deep grabens, this uncertainty is due to the limit of penetration and/or the presence of multiples which prevents us from precisely defining the limit between the pre- and syn-rift sediments on the conventionally processed lines.

In the offshore continental domain, the acoustic basement is displaced by large-offset normal faults (ca. 2–5 km, Fig. 6). The seismic facies of the basement is characterised by high amplitudes and medium to low frequency. The overlying sedimentary cover exhibits large thickness variations, being thickest in the deep fault-related grabens. In the DIM graben, the layered acoustic basement displays divergent syn-tectonic sediments (observable on the PSDM section or on the ES08 line, Figs 4 and 7), which are interpreted as syn-rift series (see below).

In the oceanic domain, the top of the acoustic basement is strongly reflective and displays a rough topography associated with numerous small-offset faults (ca. < 1.5 km, Fig. 6). The underlying seismic facies appears stratified with thick, flat and short sub-horizontal reflectors of high amplitude. The sedimentary cover has a relatively constant thickness.

In the OCT domain, the OCT ridge shows a smooth morphology (Fig. 6). The top of the basement is more reflective on the ridge flanks. The southern flank locally comprises several southward dipping divergent reflectors (ENC32, Fig. 6). On the OCT ridge flanks, the overlying sediments are either concordant with the top of the basement or show an onlap relationship.

4.2 Syn-rift sequence (Unit 1)

In the perched graben, Unit 1 (U1) lies between the top of the acoustic basement and the D1 unconformity, with a maximum thickness of 2,400 to 3,000 m (Fig. 3). U1 is characterized by discontinuous high-amplitude and low-frequency reflections that onlap onto the basement (Figs 3, 6, 7 and 8a). Chaotic facies with medium amplitudes and low frequencies can be observed at the foot of main fault scarps (Figs 3 and 8a). These might be fault-related breccias. This unit is poorly visible on the conventionally processed lines of the distal margin. It is identified on the PSDM line in the DIM graben.

The main characteristic of this unit is the wedge-shaped geometry of the reflectors. Hence, the graben infilling is asymmetric, with a systematic northward thickening toward the main normal faults. Unlike previous observations on three-channel profiles (d'Acremont *et al.* 2005), southward-thickening wedges are not observed on the studied lines (Fig. 6).

Two types of wedge are observed on the ENC34 PSDM line in the DIM graben (Figs 6b and 8c). The first type corresponds to diverging reflectors (6–8 km wide wedges), which are subsequently offset by faults. The second type corresponds to shallower and narrower wedges (2–3 km wide) ?built up/bounded by the new regularly spaced faults. These latter wedges have not suffered any subsequent deformation. This geometry is compatible with two successive block-faulting episodes: the initial deep sedimentary wedges were cut by new, closely spaced faults, which resulted in the shallow smaller wedges (Fig. 6b). The deepest wedges are poorly or not at all resolved on the conventionally processed time sections, but can be revealed by PSDM processing.

All the faults root at a common depth of about 3 km under the top of the basement (Fig. 8c), which may represent either a shallow decollement level or the base of the brittle crust.

Wedge-shaped geometries are classically related to syn-tectonic sedimentation along listric normal faults. On passive rifted margins, wedge structures are interpreted as syn-rift sediments deposited during the thinning of the continental crust. in half-grabens at the top of

blocks that are tilted along normal faults. This implies that the basement beneath such sedimentary wedges is made of continental crust, although such an interpretation may be too simplistic in continental break-up zones, where the OCT has undergone a complex morphotectonic evolution (Péron-Pinvidic *et al.* 2007). In the present study, U1 is interpreted as a syn-rift series deposited on thinned continental crust (see discussion below). Accordingly, the whole DIM graben is included in the continental domain. On this margin segment, this implies a slight southward shift of the limit of the continental domain; in this way, the limit no longer occurs in the middle part of the DIM graben, where it was initially interpreted to lie (d'Acremont *et al.* 2005; d'Acremont *et al.* 2006), but moves towards a more distal position at the seaward edge of the graben.

4.3 Syn-OCT sequence (Unit 2)

Unit 2 (U2) lies unconformably on syn-rift unit (U1) and the acoustic basement with clear onlaps (Figs 3, 7 and 8). It is bounded/?intercalated between the D1 and the D2 surfaces (Fig. 3). The curvatures of the reflectors observed on the seismic lines (Figs 6 and 7) are often accompanied by onlaps of younger less curved series onto older more curved reflectors in the underlying formations. The seismic facies shows continuous high-amplitude and low-frequency reflectors. In the perched graben, we observe chaotic facies at the foot of the fault scarp with reflection downlaps of medium amplitude and low frequency (Figs 3, 7 and 8a). U2 is only slightly deformed along small-offset normal faults connected at the roof of the basement (Fig. 7). U2 reaches a maximum thickness of 1000 m in the DIM graben.

The weak deformation and, in particular, the lack of syn-tectonic wedges, show that U2 was deposited after the main phase of syn-rift extensional tectonics. Moreover, as post-rift sediments postdate the onset of spreading, the post-rift cover is defined as the sedimentary succession lying above the oceanic crust. However, the accumulation of undeformed sediment is thicker in the DIM graben than in the oceanic basin (Fig. 6), while reflector correlations

14

show that the post-rift sequence has a constant thickness. In the DIM graben, the sediment excess under the post-rift cover makes up U2. These deposits accumulated on pre-existing relief after the activation of syn-rift faults but before the spreading. Thus, they were most likely laid down during the emplacement and deformation of the OCT. For this reason, this unit is called the syn-OCT unit.

4.4 Post-rift sequence (Units 3 to 5)

The units U3, U4 and U5 lie on oceanic crust (Figs 6, 7 and 8), and are thus considered to represent the post-rift sequence postdating the onset of spreading.

Unit 3 lies between the D2 and the D3 surfaces (Fig. 3). The boundary between U2 and U3 is conformable. The seismic facies shows continuous reflectors with interbedded chaotic facies. This unit represents the earliest sequence of post-rift sediments.

Unit 4 is intercalated between the D4 unconformity at its top and the D3 unconformity at its base (Fig. 3). The D3 unconformity is characterized by overlying onlaps (Figs 6, 7 and 8). The seismic facies show continuous low-amplitude and high-frequency reflectors.

Unit 5 lies between the seafloor and the D4 unconformity (Fig. 3). The D4 unconformity is characterized by toplaps (Fig. 7). The seismic facies displays continuous low-amplitude and high-frequency reflectors.

5 SPECIFIC SEISMIC OBSERVATIONS

5.1 Volcanic features

No volcanic features were previously identified in the study area. The new seismic data, together with recent heat flow measurements acquired during the Encens-Flux cruise (November/December 2006, Lucazeau *et al.* 2008), provide evidence of some volcanic activity on the distal margin. A very high local heat flow value (> 890 mW.m^{-2}; Lucazeau *et*

al. 2009) was recorded above the ENC34 OCT ridge (Fig. 4). This high value, together with the conical 3D morphology highlighted by the bathymetric map, is suggestive of a volcano (Figs 5a and 8d).

According to the seismic data (Figs 4 and 8d), the basement high is flanked by a series of smooth high-amplitude reflectors that correspond to large contrasts in acoustic impedance, as usually observed in volcano-sedimentary series. On the southern edge, the strong reflectors extend over about 10 km at the foot of the volcano, dipping southward with a thickening wedge-shaped geometry (1 km thick, Figs 8d and 9e). This feature suggests a volcano-sedimentary wedge. On the northern side, the strong reflectors are parallel and drape over the top of the acoustic basement. They could correspond to lava flows or sills intruded under the syn-OCT sediments.

The top of the basement of the OCT ridge displays a comparable seismic pattern with high amplitudes on all the crossing seismic lines. These high amplitude reflections are clearly associated with the volcano on the ENC34 line, and are correlated laterally in a line running parallel to the ridge, and picking out its continuity along the whole of the Ashawq-Salalah segment (Fig. 5). In the simplest case scenario, which involves a single origin for the formation of the whole ridge, this suggests that the ridge has at least a partly volcanic origin.

To constrain the emplacement chronology of the volcanic formations, we use the Encens-Sheba seismic data to study the geometry of the sedimentary series on either side of the OCT ridge. Although these data are less penetrative, they yield a better resolution of the sedimentary sequence (Fig. 7). These observations are supplemented by the other across-margin lines.

In the DIM graben, the onlaps of U2 and U3L onto the OCT ridge flank show that these units were deposited on a pre-existing syn-rift relief. The upward curvatures of the reflectors along the basement decrease up-section from U2 to U5. Onlaps on underlying more strongly curved layers show that these structures do not result only from differential compaction but also from

16

ridge uplift. The few small-offset normal faults observed above the OCT ridge flanks are possibly related to these post-rift vertical movements.

On the southern edge of the OCT ridge, the lowermost U3L shows divergent or tilted reflectors eroded at the top, consistent with an initial southward tilt of the high along the northern boundary faults (Fig. 7, CDP 1500-1700). In this unit, internal toplaps mark an erosional surface that abuts onto the basement (Fig. 7, dotted line from CDP 1950-2100). This erosional surface is not observed in the DIM graben. The overlying reflectors (U3L) are parallel to the erosional surface as well as the OCT ridge flank. Furthermore, the thickness of U3L is the same on both sides of the OCT ridge. Unless these sediments were deposited on the slope with a constant thickness, it would appear that they predate a major uplift of the basement high.

Over the OCT ridge, the U3U is thinner (Fig.7) or nonexistent (e.g. ENC32, Fig. 6) and, in some places, it is offset by faults (Figs 7 and 6 for ENC35 and ENC32 lines, respectively). U3U reflectors are clearly divergent on the southern edge of the OCT ridge (Fig. 7), indicating a continuous southward tilting and uplift of the basement during their emplacement. The southward tilt of U3L is explained by this uplift. On the southern OCT ridge flank, small-offset faults accommodate the destabilisation and sliding of U3L (Fig. 7). On the northern side, the uplift is accommodated by several normal faults, in such a way that sediment deformation is distributed in space, leading to the formation of many onlaps on ancient scarps. This results in the thinning of U3U toward the faults. On the side towards the main scarp, the sediments are not thinned, which indicates that deformation is localized on the OCT ridge.

U4 and U5 correspond to passive infilling of the grabens (Figs 7 and 10d). These reflectors onlap the basement and U3. Nevertheless, they are curved above the OCT basement high. This suggests that i) the sediments were emplaced on the paleo-relief with a constant thickness, and ii) strata were deformed after U5 (Fig. 10e). Several internal onlaps in U4 may

17

also indicate rapid and limited vertical movements on the OCT high (but none on the main scarp).

On the OCT ridge, faulting density in the sedimentary cover decreases upward and southward, the largest offset normal faults being along its northern flank. The geometry of the deposits belonging to the post-rift sequence (from U3L to U5) indicates that deformation could be coeval with the emplacement of magmatic features on the Ashawq-Salalah segment (see below).

5.2 Submarine landslide

On the margin, improvement of PSDM processing on the ENC34 line reveals a complex structure within the upper part of the horst delimiting the margin slope (Figs 4 and 8b). Whereas seismic facies are generally ?disorganised/chaotic in the basement highs of the margin, they display reflectors in the shallow southern part of this horst (Fig. 8b). Groups of short parallel reflectors with high amplitude and low frequency are shifted and tilted along small-offset faults. The faults are regularly spaced and delimit 2-km-wide tilted blocks. They dip southward and seem to connect at depth onto a south-dipping shallow low-angle feature. This fault system is about 2 km thick, extending over 15 km (Figs 5a and c), and terminates in the northern part of the DIM graben, where it is overlain by the sediments of U2.

The geometry and scale of this fault system is compatible with a destabilisation of sedimentary layers on a shallow decollement, such as a gravitational sliding. From a 3D study of this system on other seismic lines with various orientations, we can estimate the orientation of the faults (Figs 5a and c), which suggests a mean NE–SW direction of sliding with a 'top-to-the-west' sense of movement. Thus, the interpretation of a submarine landslide is supported by the kinematics of the system, which indicates sliding towards the rift axis depression.

The emplacement age of the landslide is not well constrained by the seismic data. However, the landslide mass is located under the top of the acoustic basement described in section 4.1. On all the lines, is the youngest unit observed under the top of the acoustic basement is the syn-rift unit (U1). Therefore, we propose that the submarine landslide does not contain syn-OCT sediments and that it remobilised older material, most probably syn-rift and pre-rift deposits. Accordingly, it would have occurred at the end of or after the syn-rift stage. In the DIM graben, a thick section of syn-OCT sediments (U2) displays onlaps onto the southern end of the landslide (Figs 8b and c), so we conclude that the submarine landslide occurred during late syn-rift to early OCT times.

Two layers in the stratigraphy sequence described onshore could be good candidates for such a decollement: i.e. i) the pre-rift evaporites of the Rus Formation (Late Ilerdian to Cuisian, 60 m thick) (see section 2.2) and ii) the clayey Shizar member of the syn-rift Ashawq Formation (Fig. 3). On the profile, the decollement is clearly located in the part of the tilted block composed of pre-rift sediments. Hence, the submarine landslide most likely rooted on the evaporite layer of the Rus Formation (Fig. 8b) and not into syn-rift sediments.

5.3 Deep reflections

In the oceanic domain, the PSDM ENC34 line shows a deep band of strong and discontinuous reflectors at a depth of 7.5 km (Figs 4, 6 and 8d). This band is ~ 400 m thick and attains a depth of 4 km beneath the top of the oceanic basement. While this reflective band is sub-horizontal in the southern end of the line, it displays several northward-dipping reflectors under the southern limit of the OCT domain. The character and depth of this reflective band suggest that it corresponds to the oceanic Moho.

In the OCT domain, the acoustic basement on the across-margin lines ENC32 and ENC30 displays a group of deep (down to 6 s TWTT, ca. 7 km depth) parallel strong reflectors under the southern flank of the OCT ridge (Fig. 6, ENC32). These reflectors dip southwards in

concordance with the basement top and may image a deep expression of the shallow volcanic activity on the OCT ridge as described in section 5.1.

6 DISCUSSION

6.1 Thinning mechanisms and structure of the continental crust

6.1.1 Margin structure and sense of shear

On the Ashawq-Salalah segment, syn-rift sediments are characterised by wedge-shaped geometries with a systematic thickening towards the north along one or more southward-dipping normal fault(s). The cumulate offset along these parallel faults is much larger than along the conjugate northward-dipping faults, which are less numerous. On this segment of the margin, this leads to the formation of syn-rift asymmetric grabens bounded by a major southward-dipping normal fault system.

Analogue modelling shows that conjugate normal faults join and root on the brittle–ductile transition (BDT, Fig. 9); the initial width of a rift thus depends on the brittle crust thickness. According to this modelling, the fault asymmetry indicates the sense of shear at the base of the faulted system (Faugère & Brun 1984; Vendeville *et al.* 1987; Allemand & Brun 1991; Brun & Beslier 1996). Based on the observations of Allemand & Brun (1991), the relatively narrow perched graben (16 to 19 km) would suggest a relatively shallow brittle–ductile transition in the continental crust, assuming that faults reach the BDT. Modelling, both at crustal and lithospheric scales, indicates that the shear sense on a decollement or the BDT is ?synthetic/a resultant of the sense of movement along the main normal faults. For the whole Ashawq-Salalah segment, the fault asymmetry would indicate a top-to-the south shear sense in the lower ductile crust at the margin scale during the continental break-up (Figs 9a and b).

6.1.2 Structure and formation of the DIM graben

Mantle exhumation in the OCT has been recognized on the conjugate West Iberia-Newfoundland margins (Boillot *et al.* 1987; Whitmarsh & Sawyer 1996; Chian *et al.* 1999; Whitmarsh *et al.* 2001; Tucholke *et al.* 2007). Serpentinization of mantle rocks due to contact with hydrous fluids is not just restricted to the OCT but also occurs at depth, under the highly thinned continental crust (Chian *et al.* 1999; Pérez-Gussinyé *et al.* 2001; Zelt *et al.* 2003). Numerical modelling shows that brittle deformation regimes tend to dominate in the upper lithosphere in the final stages of continental thinning (Pérez-Gussinyé & Reston 2001; Pérez-Gussinyé *et al.* 2006). The embrittlement of the entire crust allows fluids to penetrate through the crust down to the underlying mantle. On the West Iberia margin, this phenomenon would take place at a calculated stretching factor of about 4. Under the deep continental margin, the observed stretching factor is 4 to 6 , which was attained during the rifting over a time span of 7 to 25 Ma. Thus, on this margin, serpentinisation may have occurred under the wedge of thinned continental crust after it became entirely brittle.

The same approach was tentatively applied to the NE Gulf of Aden margin. Onland, receiver function analysis yields a pre-rift total crust thickness of 35 km (Tiberi *et al.* 2007). Under the DIM graben of the Ashawq-Salalah segment, a maximum crustal thickness of about 8 km can be inferred from gravity inversion (d'Acremont *et al.* 2006) and wide-angle data modelling (Watremez *et al.* 2009; Leroy *et al.* submitted) (Fig. 9e). The stretching factor is thus comprised between 4 and 5, for a maximum rifting duration of 15–18 Ma. A comparison with theoretical calculations shows that, under these conditions, the distal Gulf of Aden continental crust would become entirely brittle (see Fig. 7 in Pérez-Gussinyé & Reston 2001). Such a comparison is only relevant if the predicted crustal thickness values are valid, assuming that initial lithosphere rheologies and syn-rift strain rates are comparable in both the Iberian and Gulf of Aden rifted areas. This may be a reasonable assumption: i) for the Gulf of Aden area, the initial lithosphere is typical of an 'old collapsed orogen' and a crustal thickness of 32 km thick may be adequate to a

first order of approximation; ii) the stretching factor (4 to 5) and rift duration (15–18 Ma) are comparable to those of West Iberia. Accordingly, the seismic lower crust under the DIM graben may be made up of partly serpentinized mantle (Fig. 9).

Moreover, complex faulting geometries have been observed on deep magma-poor margins where extreme crustal thinning has occurred (e.g. Manatschal 2004; Reston & Pérez-Gussinyé 2007). These geometries result from several interacting processes: i) the superposition of several generations of faults due to the flattening and ?locking up/sealing of initially steep faults, and ii) the formation of detachments along the crust–mantle boundary in relation to mantle serpentinisation, with some of these decollements taking place at the top of the serpentinised mantle under a highly thinned (ca. 3 km thick) continental crust (Boillot *et al.* 1995; Brun & Beslier 1996; Pérez-Gussinyé *et al.* 2001; Manatschal 2004; Reston & Pérez-Gussinyé 2007).

Similarly, the DIM graben displays a polyphase faulting of the thin upper faulted crust, where two wedge systems of different scales are superposed (Fig. 8c). The wider spacing (6–8 km) of the earliest faults implies that they formed in a brittle crust that was thicker than the present-day crust, as suggested by analogue modelling (Vendeville *et al.* 1987). This is consistent with an ongoing thinning of the deep margin, whereby the localisation of deformation leads to break-up (Figs 9a and b). The latest generation of closely-spaced faults (2–3 km) indicates a final thickness of nearly 3 km for the upper faulted layer (Fig. 8c). These faults may root on a decollement at the top of the partly serpentinized mantle. Such a decollement would imply a stretching factor higher than 10 in the continental crust, which is far more than needed for the crust to be entirely brittle, allowing for the serpentinization of the underlying mantle. In that case, the switch from the widely to the closely spaced fault systems may be coeval with the complete embrittlement of the crust and the beginning of mantle serpentinisation. Such a decollement is described by Reston (1996) for the S reflection on the deep Galician margin. Although similarities exist between the deep Galician margin and the

DIM graben, the MCS data do not indicate a strong reflector at the rooting level of the normal faults under the DIM graben. Consequently, we consider that the deep seismic crust under the DIM graben could be made up either of thinned lower continental crust or partly serpentinised mantle.

It noteworthy that the set of faults is asymmetric (all the sedimentary wedges thicken toward the north), suggesting a continuous 'top-to-the-south' sense of shear at the base of the crustal tilted blocks. However, this does not preclude the possible symmetry of the whole DIM graben, whose southern part today lies on the conjugate margin.

Some authors suggest that, on the distal south Iberia abyssal plain (SIAP), syn-tectonic sediments may have been deposited over exhumed mantle during the OCT deformation, before or at the onset of oceanic spreading (Beslier *et al.* 1996; Péron-Pinvidic *et al.* 2007). The deformation is thus due to widening of the OCT by a tectonically dominated extension of the exhumed mantle. However, the thickness of the syn-tectonic units in the DIM graben favours the interpretation of U1 as a syn-rift unit, implying that the DIM graben is part of the continental domain. In the study area, we observe two syn-tectonic units: (1) U1, associated with faulting and tilting of basement blocks, and (2) U2, which is only weakly deformed. Each of these units are 1 km thick in the DIM graben. Considering the narrowness of the OCT (15 km), and assuming that a total thickness of 2 km (U1 plus U2 thicknesses) was deposited during OCT widening, this would imply a very high sedimentation rate during the deformation (~ 1 mm/year). However, average vertical clastic sedimentation rates in the Red Sea are estimated at 0.08 mm/year since the early Miocene (Davison *et al.* 1998). In our interpretation, the deformation would be localised in the OCT during the deposition of U2 (see section 3.3), which would explain the weak deformation of this unit in the continental domain. Moreover, by comparing the polyphase evolution of the DIM graben with other distal magma-poor margins, as discussed above, we favour the interpretation of U1 as syn-rift sediments deposited on extremely thinned continental crust.

According to our interpretation of the Ashawq-Salalah segment, (1) the oceanward limit of the continental domain is located on the southern edge of the DIM graben, where we observe the youngest occurrence of syn-rift sediments, (2) the newly defined OCT is narrow (ca. 15 km) and restricted to the so-called OCT ridge, (3) the distal continental crust seems very thin and could have led to mantle serpentinization and exhumation, (4) the D1 unconformity is associated with the complete break-up of the continental crust, while the D2 unconformity is coeval with the onset of seafloor spreading, with U2 corresponding to the only syn-OCT series (see Fig. 3).

This interpretation of the Ashawq-Salalah segment does not rule out lateral variations in the basement geometry or the nature of the OCT along the whole deep margin of the north-eastern Gulf of Aden (Leroy *et al.* submitted.).

6.2 Structure and nature of the OCT: syn-rift mantle exhumation and post-rift volcanism

Several seismic features on the MCS data are interpreted as being related to volcanic activity in the OCT area: the presence of a volcano (Fig. 5a), high heat flow (Lucazeau *et al.* 2009), volcanic flows or sills, volcano-sedimentary wedges (Figs 6 and 8d) and a deep set of strong oceanward dipping reflectors (ENC32, Fig. 6). The continuity of the OCT ridge and related volcanic features suggests a volcanic affinity along the whole OCT ridge in the Ashawq-Salalah segment (see section 5.1). These volcanic features could be explained by intrusions of magmas derived from partial melting of the mantle before the onset of true spreading at anomaly 5d. Nevertheless, the detailed study of the sedimentary cover of the OCT ridge shows that the present ridge morphology was partly acquired over a long time span following the onset of oceanic crust spreading (from 17.6 Ma to ca. 5 Ma at least until the D3 unconformity, or possibly up to the present day).

On line ENC34, the oldest 5d magnetic anomaly is superposed onto a volcano-sedimentary wedge, which indicates that it formed during or after the onset of spreading (Fig. 7). As the 5d anomaly is observed all along the margin and has a clear oceanic magnetic anomaly signature (Leroy *et al.* 2004), we assume that it is recorded by the oceanic crust and not by the volcanic material. Moreover, the volcano-sedimentary wedge is not thick enough (1 km) to disturb the signature of the magnetic anomaly. On the northern side of the ridge (Fig. 8c), we cannot establish the emplacement chronology with certainty, even in relative terms, since any post-rift intrusive volcanics are mostly interbedded in the sedimentary succession (e.g. Karner & Shillington 2005).

In the following, we present the relative timing of development of the OCT ridge as established from analysis of the sedimentary records on line ES08 (see section 5.1 and Figs 7, 9 and 10) and observations made on other across-margin lines of the segment:

(1) Faults are initiated during rifting and pre-condition the structure of the OCT ridge (Figs. 9a and b). This proto-ridge is possibly made up of partly serpentinised mantle.

(2) OCT sediments (U2) and U3L fill the paleo-relief (Fig. 9c). Their poorly developed divergent bedding indicates a restricted syn-depositional displacement on the boundary faults (Figs 8 and 10).

(3) An initial slight southward tilt of the basement high occurs at the very beginning of post-rift sedimentation (base of U3L). The formation of the oceanward-thickening volcano-sedimentary wedge, which underlies this series at the top of the acoustic basement, most probably accompanies this initial event (Figs 8d and 10a).

(4) Subsequent erosion occurs, but is not well constrained (Fig. 10a). The U3L internal erosional surface is not observed in the DIM graben. Nevertheless, since the erosional surface and the southern edge are horizontally aligned, it could have affected the basement high. This erosion could be of two origins: i) the basement high has sufficient relief to generate sliding

25

on its flank, which leads to erosion of the underlying sediments; ii) uplift induces local emergence of the OCT high. In both cases, the underlying strata would need to be tilted southward before the erosion.

(5) Growth of the basement high is interrupted as horizontal parallel layers are emplaced over the whole area (U3L) (Figs 7 and 10b).

(6) Major growth of the basement high occurs during deposition of U3U (Fig. 10c).

(7) Graben filling is sometimes accompanied by slight vertical movements of the OCT high (Figs 10d and e). U4 and U5 correspond to passive infilling of the grabens (Figs 7 and 10d). The possible recent uplift (Fig. 10e) could be related to i) recent magmatic activity (100 ky), best explaining the high heat flow value measured at the top of the OCT basement high (Lucazeau *et al.* 2009), as well as ii) persistent thermal effects on this margin associated with small-scale convection processes at the edge, between the thick cold continental lithosphere and the thin hot oceanic lithosphere (Lucazeau *et al.* 2008). Thus, we propose that the present-day OCT ridge morphology was partly formed during post-rift times in relation to volcanic activity in the OCT after the onset of oceanic spreading. These observations support the hypotheses based on the interpretation of the seismic lines and are corroborated by the presence of an anomalous magmatic activity at the western segment of the spreading ridge, corresponding to the continental Ashawq-Salalah segment (d'Acremont *et al.* submitted). A plume-ridge interaction model, involving a channelized flow of Afar plume material along the Aden-Sheba ridge system, could account for the feeding of this volcanic activity as from the earliest stages of OCT emplacement (Leroy *et al.* in rev).

Accordingly, two processes appear to be responsible for the building up of the OCT ridge: i) possible emplacement of exhumed mantle during OCT formation and an early structural development of the basement, as inferred from the oldest sediments in the DIM graben, and ii) post-rift magmatic activity, responsible for the post-rift growth of the ridge. Nevertheless, it

remains impossible to form a clear picture of the initial structure of the OCT, before or during the initial stages of oceanic accretion.

The formation of the OCT on this segment is thus the result of a long and complex interaction of tectono-metamorphic and magmatic events which have changed not only the morphology, but also the internal structure of the OCT. The deep strong intra-crustal reflectors clearly seen on the ENC30 and ENC32 lines (Fig. 6) could be due to magmatic features that are possibly contemporaneous with the volcano-sedimentary wedge. This hypothesis implies a strong reduction in the amount of serpentinised mantle in the 'seismic' crust, not only because of massive magmatic intrusions, but also because serpentinite is not stable at temperatures higher than 500°C (Martin & Fyfe 1970; Escartín *et al.* 1997; Früh-Green *et al.* 2004). A higher temperature results in recrystallization of olivine. Thus, the high temperature may have at least partly erased the serpentinisation in the exhumed mantle. On this segment of the margin, the study of the present-day OCT cannot document accurately the final stages of continental break-up and OCT formation on magma-poor margins.

6.3 Characteristics of the oceanic crust

In the oceanic domain of the Ashawq-Salalah segment, two types of reflection have been observed: Moho reflections and deep reflections located beneath the Moho.

In the PSDM ENC34 section, Moho reflections are only observed in the oceanic domain (Figs 4 and 6). They define an oceanic crust as thick as 4–5 km, in good agreement with the 3D gravity inversion (d'Acremont *et al.* 2006). This is relatively thin compared to the standard oceanic crust (7.1+/-0.8 km or 5 to 8.5 km) defined by White (1992) from a compilation of seismic results. Thin oceanic crust is commonly recorded near the OCT, for example: on the Newfoundland margin (2–4 km, Shillington *et al.* 2006; Tucholke *et al.* 2007), in the Cayman Trough (~ 5 km, Leroy *et al.* 1996) and on the southern Atlantic margins (Contrucci *et al.* 2004).

The second seismic pattern corresponds to strong discontinuous deep reflectors comprised of several successive landward-dipping features (Fig. 6 on ENC34 profile and Fig. 8d). Similar reflector geometries found on other margins are interpreted in different ways.

(1) Low-angle detachment affecting the conjugate margins from within the continental mantle, with a general dip towards the continent (as observed in the West Iberia margin, Reston 1990; Pickup *et al.* 1996). These detachment faults allow decoupling between the updoming sub-continental mantle and the stretched continental crust.

(2) Detachment faults linked to the oceanic ridge lead to the exhumation of lower crustal and/or serpentinized upper mantle rocks at shallow depths (Schroeder & John 2004; deMartin *et al.* 2007).

(3) Faults shifting the whole oceanic crust, with a dip towards the continent or towards the ocean (Wilson *et al.* 2003).

(4) Lithological layering of magmatic origin is developed in the lower crust near the oceanic ridge (Ranero *et al.* 1997; Reston et al. 1999; Reston et al. 2004).

In our case, the dipping reflections are located beneath the oceanic crust, which suggests shear zones that affect the sub-continental mantle (and possibly the new oceanic mantle) until the spreading becomes completely effective. Such shear zones would be consistent with several models of extension (Nagel & Buck 2007; Weinberg et al. 2007). Nevertheless, the broad pattern and brightness of the reflections suggest a possible magmatic origin or overprinting. Indeed, sharp tectonic boundaries such as localised mantle/crust detachment faults could give rise to simple reflections that are more continuous (Reston 1996; Hölker et al. 2002).

6.4 Tectono-sedimentary evolution of the Ashawq-Salalah segment

All the observations and interpretations from the seismic lines are brought together here to propose a tectono-stratigraphic model of evolution for the western segment of the margin (Fig. 9). Because of the realistic geometries and depth of structures observed on the ENC34

PSDM section, we focus our schematic evolution on this profile. We also attempt to construct a chronological interpretation of the sedimentary sequences identified in the deep margin in relation to the onshore observations and dating results (Roger *et al.* 1989; Leroy *et al.* 2007), which is summarised in Figure 3.

6.4.1 Syn-rift stage (Fig. 9a)

The rifting (Fig. 9a) is marked by nine large offset normal faults that root at a common depth, possibly corresponding to the brittle–ductile transition (BDT). They tilt the pre-rift sediments and the underlying basement and result in asymmetric syn-rift grabens as wide as 5-10 km. The size of the eight tilted blocks decreases oceanward. Below the DIM graben, the tilted blocks are 6-8 km wide. The decreasing size of fault blocks farther from the margin implies a temporal progression of deformation and, therefore, a temporal migration of rifting from proximal to distal parts of the margin. In that case, the proximal syn-rift unit could be younger than the distal syn-rift unit, and our correlation may relate to the kind of deformation rather than the time at which it took place.

6.4.2 Late syn-rift stage (Fig. 9b)

The continuous thinning of the continental crust leads to the formation of more closely spaced faults (2–3 km) and blocks of shorter wavelengths on the deep margin where the extension is localized (Fig. 9b). The extreme thinning and possible complete embrittlement of the continental crust may allow serpentinization of the underlying mantle. Onshore, the coeval Mughsayl Formation (Fig. 3) records an acceleration of the subsidence during Aquitanian times. Later, Gilbert deltas, probably Burdigalian in age, indicate a fast regression resulting from relatively fast margin uplift (Leroy *et al.* 2007).

6.4.3 OCT time (Fig. 9c)

As extension proceeds and uplift occurs onshore, the differential vertical movement between proximal and distal parts of the margin increases the slope of the margin. The submarine landslide observed on the southernmost continental tilted block probably occurred at this time along a decollement layer in the pre-rift series (Figs 8b and 9c).

With ongoing extension, complete break-up of the continental crust takes place in the southern part of the DIM graben, where the crust is thinnest. The OCT may be created by exhumation of underlying partly serpentinized mantle in the break-up zone. The extension is then localised in the OCT, where the exhumed mantle becomes stretched before or during incipient spreading. During formation of the OCT, flat syn-OCT sediments are deposited in the DIM and perched grabens (Fig. 9c). The syn-OCT unit predates the initiation of spreading (17.6 Ma) since it is not emplaced on oceanic crust (Fig. 9c). Onshore, it is correlated with a sedimentary gap between syn- and post-rift onshore series that we interpret as resulting from final syn-rift uplift (Fig. 3).

6.4.4 Initiation of spreading (Fig. 9d) and post-rift stage (Fig. 9e)

The OCT widening ceases when true oceanic spreading begins (anomaly 5d, 17.6 Ma) (Fig. 9d). The post-rift stage is marked by several magmatic events (Fig. 9e). Shortly after the onset of spreading, an initial southward tilt of the OCT ridge is recorded by the basal U3L (Fig. 7). This is accompanied by northward-facing faults and the emplacement of the southern volcano-sedimentary wedge. The volcanic flows or sills observed in the north of the basement high could be coeval with this event. The proximal part of the margin, currently cropping out onshore, is still exposed and being eroded at this time. It is possible that uplift could have led to emergence of the whole margin as suggested by the erosional surface cutting down into the U3L, as described in section 5.2 (profile ES08, CDP number 2000 and higher on Fig. 7). Alternatively, erosion may result from sub-marine flows or sliding in relation to the localized

extent of this surface. The major post-rift growth of the OCT ridge occurs during the deposition of U3U (Fig. 10c). Emplacement of the ENC34 volcano is probably progressive and related to several volcanic events. We correlate U3 to the onshore Adawnib and Nar Formations, which mark a subsidence of the margin during the Langhian, followed by emergence from Serravallian times onward (Fig. 3). Offshore, U4 and U5 display sub-marine erosional unconformities which provide evidence for the subsidence of the grabens and indicate vertical movements during the post-rift stage. The D3 unconformity (Fig. 3) could be related to the final emergence of the proximal margin farther onshore during the Pliocene (Platel *et al.* 1992). Hence, vertical movements occur both onshore and offshore over the whole margin during the post-rift stage.

7 CONCLUSIONS

We propose here a continental break-up history for the deep magma-poor margin of the north-eastern Gulf of Aden. The proposed evolution from rifting to spreading of the Ashawq-Salalah segment is correlated with data from the proximal margin cropping out onshore. This correlation is based on the assumption that the generally detrital distal offshore sedimentary succession may be poorly developed or missing when onshore sedimentation is significant, and *vice versa*. Moreover, the syn-rift series may be younger toward the distal margin. In spite of these assumptions, and because there are no offshore drilling data from this margin segment, this correlation leads to further interpretations of the offshore features.

During the syn-rift stage (late Priabonian to early Burdigalian), faults may reach the brittle–ductile transition, which would exhibit a top-to-south shear direction. The development of faulting indicates a localisation of the deformation and thinning at the crustal scale in the DIM graben (DIstal Margin graben). This extremely thinned continental crust conditioned the future emplacement of the OCT. The coeval onshore syn-rift formations record an acceleration of the subsidence and, subsequently, the onset of fast margin uplift.

During formation of the OCT (middle Burdigalian), uplift related to onland erosion could have induced a submarine landslide on the top of the southernmost horst of the continental domain. This sliding could have rooted on the pre-rift evaporitic Rus Formation. In the DIM graben, the strain localisation shifted southward, towards the location of the present-day OCT ridge, where continental break-up finally occurred with the creation of the paleo-ridge. Since the crust is extremely thinned, we suggest that the OCT is at least partly composed of exhumed serpentinized mantle .

The oceanic crust has a thickness of 4–5 km, which is relatively thin. Deep crustal reflections in the oceanic transitional mantle could represent the imprints of continentward detachments within the mantle, decoupling first the crust and mantle, then the serpentinized and non-serpentinised upper mantle during extension.

During post-rift times (late Burdigalian [17.6 Ma] to present), magmatic activity possibly took place in the OCT domain, where the lithosphere is thinnest, towards the end of OCT formation. Such magmatic activity would explain the late growth of the proto-OCT ridge. Hence, the formation of the OCT on this segment of the margin is the result of a long and complex interaction of tectono-metamorphic and magmatic events. Therefore, the present-day nature of the OCT could correspond to a combination of exhumed serpentinized mantle and late-stage magmatic intrusions. The final stages of continental break-up and OCT formation on magma-poor margins cannot be adequately documented by the magmatic overprint on the initial structural development of the OCT in this segment of the margin, or by the study of the present-day OCT.

ACKNOWLEDGMENTS

REFERENCES

Agudelo, W., 2005. Imagerie sismique quantitative de la marge convergente d'Equateur-Colombie : Application des méthodes tomographiques aux données de sismique réflexion multitrace et réfraction-réflexion grand-angle des campagnes SISTEUR et SALIERI, PhD thesis, Université Paris VI, France.

Al-Yahya, K.M., 1987. Velocity analysis by iterative profile migration, PhD thesis, Stanford University.

Allemand, P. & Brun, J.-P., 1991. Width of continental rifts and rheological layering of the lithosphere, *Tectonophysics,* 188**,** 63-69.

Bellahsen, N., Fournier, M., d'Acremont, E., Leroy, S. & Daniel, J.-M., 2006. Fault reactivation and rift localization: the northeastern Gulf of Aden margin, *Tectonics,* 25**,** doi:10.1029/2004TC001626.

Beslier, M.-O., Cornen, G. & Girardeau, J., 1996. Tectono-metamorphic evolution of peridotites from the ocean/ continent transition of the Iberia abyssal plain margin. *in Proc. ODP, Sci. Results*, pp. 397-341, eds. Whitmarsh, R. B., Sawyer, D. S., Klaus, A. & Masson, D. G.

Boillot, G., Beslier, M.-O. & Girardeau, J., 1995. Nature, structure and evolution of the ocean-continent boundary: the lesson of the West Galicia Margin (Spain). *in Rifted Ocean-Continent Boundaries*, pp. 219-229, ed. Banda, E., Kluwer Academic Publishers.

Boillot, G., Recq, M., Winterer, E.L., Meyer, A.W., Applegate, J., Baltuck, M., Bergen, J.A., Comas, M.C., Davies, T.A., Dunham, K., Evans, C.A., Girardeau, J., Goldberg, G., Haggerty, J., Jansa, L.F., Johnson, J.A., Kasahara, J., Loreau, J.P., Luna-Sierra, E.,

Moullade, M., Ogg, J., Sarti, M., Thurow, J. & Williamson, M., 1987. Tectonic denudation of the upper mantle along passive margins: a model based on drilling results (ODP leg 103, western Galicia margin, Spain), *Tectonophysics,* 132**,** 335-342.

Bott, W.F., Smith, B.A., Oakes, G., Sikander, A.H. & Ibrahim, A.I., 1992. The tectonic framework and regional hydrocarbon, prospectivity of the Gulf of Aden, *J. Pet. Geol.,* 15**,** 211–243.

Brun, J.-P. & Beslier, M.-O., 1996. Mantle exhumation at passive margins, *Earth Planet. Sci. Lett.,* 142**,** 161-173.

Chian, D., Louden, K.E., Minshull, T.A. & Whitmarsh, R.B., 1999. Deep structure of the ocean-continent transition in the southern Iberia Abyssal plain from seismic refraction profiles: Ocean Drilling Program (Legs 149 and 173) transect, *J. Geophys. Res.,* 104**,** 7443-7462.

Clark, S.A., Sawyer, D.S., Jr., J.A.A., Christeson, G.L. & Nakamura, Y., 2007. Characterizing the Galicia Bank-Southern Iberia Abyssal Plain rifted margin segment boundary using multichannel seismic and ocean bottom seismometer data, *J. Geophys. Res.,* 112, B03**,** 17 p.

Contrucci, I., Matias, L., Moulin, M., Géli, L., Klingelhofer, F., Nouzé, H., Aslanian, D., Olivet, J.L., Réhault, J.P. & Sibuet, J.C., 2004. Deep structure of the West African continental margin (Congo, Zaïre, Angola), between 5°S and 8°S, from reflection/refraction seismics and gravity data, *Geophys. J. Int.,* 158**,** 529-553.

d'Acremont, E., Leroy, S., Maia, M., Patriat, P., Beslier Marie, O., Bellahsen, N., Fournier, M. & Gente, P., 2006. Structure and evolution of the eastern Gulf of Aden; insights from magnetic and gravity data (Encens-Sheba MD117 cruise), *Geophys. J. Int.,* 165**,** 786-803.

d'Acremont, E., Leroy, S., Beslier, M.-O., Bellahsen, N., Fournier, M., Robin, C., Maia, M. & Gente, P., 2005. Structure and evolution of the eastern Gulf of Aden conjugate margins from seismic reflection data, *Geophys. J. Int.,* 160**,** 869-890.

d'Acremont, E., Leroy, S., Maia, M., Gente, P. & Autin, J., subm., Volcanism, jump and propagation on the Sheba Ridge, eastern Gulf of Aden: Segmentation evolution and implications for oceanic accretion processes *Geophys. J. Int.*

Dauteuil, O., Huchon, P., Quemeneur, F. & Souriot, T., 2001. Propagation of an oblique spreading center: the western Gulf of Aden, *Tectonophysics,* 332**,** 423- 442.

Davison, I., Tatnell, M.R., Owen, L.A., Jenkins, G. & Baker, J., 1998. Tectonic geomorphology and rates of crustal processes along the Red Sea margin, north-west Yemen. *in Sedimentation and tectonics in rift basins: Red Sea–Gulf of Aden*, pp. 595–612, eds. Purser, B. H. & Bosence, D. W. J. Chapman & Hall, London.

deMartin, B.J., Sohn, R.A., Pablo Canales, J. & Humphris, S.E., 2007. Kinematics and geometry of active detachment faulting beneath the Trans-Atlantic Geotraverse (TAG) hydrothermal field on the Mid-Atlantic Ridge, *Geology,* 35**,** 711.

Ebinger, C.J. & Sleep, N.H., 1998. Cenozoic magmatism throughout east African resulting from impact of a single plume, *Nature,* 395**,** 788-791.

Escartín, J., Hirth, G. & Evans, B., 1997. Effects of serpentinisation on the lithospheric strength and the style of normal faulting at slow-spreading ridges., *Earth Planet. Sci. Lett.,* 151**,** 181-189.

Fantozzi, P.L. & Sgavetti, M., 1998. Tectonic and sedimentary evolution of the eastern Gulf of Aden continental margins: new structural and stratigraphic data from Somalia and Yemen. *in Sedimentation and tectonics in rift basins: Red Sea–Gulf of Aden*, pp. 56-76, eds. Purser, B. H. & Bosence, D. W. J., Chapman & Hall, London.

Faugère, E. & Brun, J.P., 1984. Modelisation experimentale de la distension continentale, *C.R. Acad. Sci., Ser. IIa: Sci. Terre,* 229**,** 365-370.

Fournier, M., Bellahsen, N., Fabbri, O. & Gunnell, Y., 2004. Oblique rifting and segmentation of the NE Gulf of Aden passive margin, *Geochem. Geophys. Geosyst.,* 5**,** 24 p.

Fournier, M., Patriat, P. & Leroy, S., 2001. Reappraisal of the Arabia-India-Somalia triple junction kinematics, *Earth Planet. Sci. Lett.,* 189**,** 103-114.

Fournier, M., Petit, C., Chamot-Rooke, N., Fabbri, O., Huchon, P., Maillot, B. & Lepvrier, C., 2008. Do ridge-ridge-fault triple junctions exist on Earth? Evidence from the Aden-Owen-Carlsberg junction in the NW Indian Ocean, *Basin Research,* 20, 4**,** 575-590.

Früh-Green, G.L., Connolly, J.A.D., Plas, A., Kelley, D.S. & Grobety, B., 2004. Serpentinization of oceanic peridotites: Implications for geochemical cycles and biological activity, *Geophys. mono.,* 144**,** 119-136.

George, R., Rogers, N. & Kelley, S., 1998. Earliest magmatism in Ethiopia: Evidence for two mantle plumes in one flood basalt province, *Geology,* 26**,** 923-926.

Hébert, H., Deplus, C., Huchon, P., Khanbari, K. & Audin, L., 2001. Lithospheric structure of a nascent spreading ridge inferred from gravity data: The western Gulf of Aden, *J. Geophys. Res.,* 106**,** 26345-26363.

Hofmann, C., Courtillot, V., Féraud, G., Rochette, P., Yirgu, E., Kefeto, E. & Pik, R., 1997. Timing of the Ethiopian flood basalt event and implications for plume birth and global change., *Nature,* 389**,** 838- 841.

Hoelker, A.B., Holliger, K., Manatschal, G. & Anselmetti, F., 2002. Seismic reflectivity of detachment faults of the Iberian and Tethyan distal continental margins based on geological and petrophysical data, *Tectonophysics,* 350, 127-156.

Huchon, P. & Khanbari, K., 2003. Rotation of the syn-rift stress field of the northern Gulf of Aden margin, Yemen, *Tectonophysics,* 364**,** 147-166.

Huismans, R.S. & Beaumont, C., 2008. Complex rifted continental margins explained by dynamical models of depth-dependent lithospheric extension, *Geology,* 36**,** 163–166.

Jestin, F., Huchon, P. & Gaulier, J.M., 1994. The Somalia plate and the East African Rift System: present kinematics., *Geophys. J. Int.,* 116**,** 637- 654.

Karner, G.D. & Shillington, D.J., 2005. Basalt sills of the U reflector, Newfoundland Basin: A serendipitous dating technique, *Geology,* 33**,** 985–988.

Kenea, N.H., Ebinger, C.J. & Rex, D.C., 2001. Late Oligocene volcanism and extension in the southern Red Sea Hills, Sudan, *J. Geol. Soc. London* 158**,** 285-294.

Lavier, L.L. & Manatschal, G., 2006. A mechanism to thin the continental lithosphere at magma-poor margins, *Nature,* 440**,** 324-328.

Lepvrier, C., Fournier, M., Bérard, T. & Roger, J., 2002. Cenozoic extension in coastal Dhofar (southern Oman): implications on the oblique rifting of the Gulf of Aden, *Tectonophysics,* 357**,** 279– 293.

Leroy, S., Ebinger, C., d'Acremont, E., Stuart, G., Al-Lazki, A., Tiberi, C., Autin, J., Watremez, L., Beslier, M.-O., Bellahsen, N., Lucazeau, F., Perrot, J., Mouthereau, F., Courrèges, E., Huchon, P., Rouzo, S., Bahalaf, S., Sholan, J., Unternehr, P., Hello, Y., Anglade, A., Desprez, O., Beguery, L., Aouji, O., Daniel, R., Al-Toubi, K. & Sage, F., 2006. The onshore-offshore ENCENS project: Imaging the stretching/thinning of the continental lithosphere and inception of oceanic spreading in the eastern Gulf of Aden. *in American Geophysical Union, 2006 Fall Meeting, abstract #T53A-1567*, San Francisco.

Leroy, S., Gente, P., Fournier, M., d'Acremont, E., Patriat, P., Beslier, M.-O., Bellahsen, N., Maia, M., Blais, A., Perrot, J., Al-Kathiri, A., Merkouriev, S., Fleury, J.-M., Ruellan, P.-Y., Lepvrier, C. & Huchon, P., 2004. From rifting to spreading in the eastern Gulf of Aden: a geophysical survey of a young oceanic basin from margin to margin, *Terra Nova,* 16**,** 185-192.

Leroy, S., Lucazeau, F., d'Acremont, E., Watremez, L., Autin, J., Rouzo, S., Bellahsen, N., Ebinger, C., Beslier, M.-O., Tiberi, C., Perrot, J., Razin, P., Stuart, G., Al-Lazki, A., Al-Toubi, K., Bache, F., Bonneville, A., Goutorbe, B., Rolandone, F., Huchon, P., Unternehr, P. & Khanbari, K., subm. Contrasted styles of rifting in the eastern Gulf of Aden.

Leroy, S., d'Acremont, E., Tiberi, C., Basuyau, C., Autin, J. & Lucazeau, F., in rev. Recent off-axis volcanism in the eastern Gulf of Aden: implications for plume-ridge interactions, *Earth Planet. Sci. Lett.*

Leroy, S., Lucazeau, F., Razin, P., Manatschal, G. & YOCMAL team, 2007. Young Conjugate Margins Laboratory in the Gulf of Aden: the YOCMAL project. *in American Geophysical Union, 2007 Fall Meeting, abstract #T41A-0350*, San Francisco.

Leroy, S., Mercier de Lépinay, B., Mauffret, A. & Pubellier, M., 1996. Structural and Tectonic evolution of the Eastern Cayman trough (Caribbean Sea) from seismic reflection data, *Am. Assoc. Pet. Geol. Bull.,* 80**,** 222-247.

Lucazeau, F., Leroy, S., Autin, J., Bonneville, A., Goutorbe, B., Rolandone, F., d'Acremont, E., Watremez, L., Düsünur, D. & Huchon, P., 2009. Post-Rift Volcanism and high heat-flow at the Ocean-Continent Transition of the Gulf of Aden, *Terra Nova,* **21** (4), 285-292.

Lucazeau, F., Leroy, S., Bonneville, A., Goutorbe, B., Rolandone, F., d'Acremont, E., Watremez, L., Düsünur, D., Tuchais, P., Huchon, P., Bellahsen, N. & Al-Toubi, K., 2008. Persistent thermal activity at the Eastern Gulf of Aden after continental break-up, *Nature geosci.,* advance online publication**,** doi:10.1038/ngeo1359.

Manatschal, G., 2004. New models for evolution of magma-poor rifted margins based on a review of data and concepts from West Iberia and the Alps, *Int. J. Earth Sci.,* 93**,** 432-466.

Manighetti, I., Tapponnier, P., Courtillot, V., Gruszow, S. & Gillot, P., 1997. Propagation of rifting along the Arabia-Somalia plate boundary: the Gulfs of Aden and Tadjoura, *J. Geophys. Res.,* 102**,** 2681-2710.

Manighetti, I., Tapponnier, P., Gillot, P., Jacques, E., Courtillot, V., Armijo, R., Ruegg, J.C. & King, G., 1998. Propagation of rifting along the Arabia-Somalia plate boundary: Into Afar, *J. Geophys. Res.,* 103**,** 4947-4974.

Martin, B. & Fyfe, W.S., 1970. Some experimental and theoretical observations on the kinetics of hydration reactions with particular reference to serpentinization, *Chem. Geol.,* 6**,** 185–202.

McKenzie, D., 1978. Some remarks on the development of sedimentary basins, *Earth Planet. Sci. Lett.,* 40**,** 25-42.

Mercolli, I., Briner, A.P., Frei, R., Schönberg, R., Nägler, T.F., Kramers, J. & Peters, T., 2006. Lithostratigraphy and geochronology of the Neoproterozoic crystalline basement of Salalah, Dhofar, Sultanate of Oman, *Precamb. Res.,* 145**,** 182-206.

Nagel, T. & Buck, W., 2007. Control of rheological stratification on rifting geometry: a symmetric model resolving the upper plate paradox, *Int. J. Earth Sci.,* 96**,** 1047-1057.

Operto, S., Lambaré, G., Podvin, P., Thierry, P. & Noble, M., 2003. 3-d ray+born migration/inversion - part 2: Application to the SEG/EAGE overthrust experiment, *Geophysics,* 68**,** 1357-1370.

Pérez-Gussinyé, M., Morgan, J.P., Reston, T.J. & Ranero, C.R., 2006. The rift to drift transition at non-volcanic margins: Insights from numerical modelling, *Earth Planet. Sci. Lett.,* 244**,** 458-473.

Pérez-Gussinyé, M. & Reston, T.J., 2001. Rheological evolution during extension at nonvolcanic rifted margins; onset of serpentinization and development of detachments leading to continental breakup, *J. Geophys. Res.,* 106**,** 3961-3975.

Pérez-Gussinyé, M., Reston, T.J. & Phipps, M.J., 2001. Serpentinization and magmatism during extension at non-volcanic margins: the effect of initial lithospheric structure, *Geol. Soc. Spec. Publ.,* 187**,** 551-576.

Péron-Pinvidic, G., Manatschal, G., Minshull, T.A. & Sawyer, D.S., 2007. Tectonosedimentary evolution of the deep Iberia-Newfoundland margins: Evidence for a complex breakup history, *Tectonics,* 26**,** doi: 10.1029/2006TC001970.

Pickup, S.L.B., Whitmarsh, R.B., Fowler, C.M.R. & Reston, T.J., 1996. Insights into the nature of the ocean-continent transition off West Iberia from a deep multichanel seismic reflection profile, *Geology,* 24**,** 1079-1082.

Platel, J.P. & Roger, J., 1989. Evolution dynamique du Dhofar (Sultanat d'Oman) pendant le Crétacé et le Tertiaire en relation avec l'ouverture du Golfe d'Aden, *Bull. Soc. Geol. Fr.,* 8**,** 253-263.

Platel, J.P., Roger, J., Peters, T., Mercolli, I., Kramers, J.D. & Le Métour, J., 1992. Geological Map of Salalah (1/250 000), Sultanate of Oman; sheet NE 40-09, Ministry of Petroleum and Minerals, Directorate General of Minerals, Oman.

Ranero, C.R., Banda, E. & Buhl, P., 1997. The crustal structure of the Canary Basin: Accretion processes at slow spreading centers, *J. Geophys. Res.,* 102**,** 10185-10201.

Reston, T. & Pérez-Gussinyé, M., 2007. Lithospheric extension from rifting to continental breakup at magma-poor margins: rheology, serpentinisation and symmetry, *Int. J. Earth Sci.,* 96**,** 1033-1046.

Reston, T., Ranero, C.R. & Belykh, I., 1999. The structure of Cretaceous oceanic crust of the NW Pacific: Constraints on processes at fast spreading centers, *J. Geophys. Res.,* 104**,** 629-644.

Reston, T.J., 1990. Mantle shear zones and the evolution of the northern North Sea basin, *Geology,* 18**,** 272-275.

Reston, T.J., 1996. The S reflector west of Galicia: the seismic signature of a detachment fault, *Geophys. J. Int.,* 127**,** 230-244.

Reston, T.J., Gaw, V., Pennell, J., Klaeschen, D., Stubenrauch, A. & Walker, I., 2004. Extreme crustal thinning in the south Porcupine Basin and the nature of the Porcupine Median High: implications for the formation of non-volcanic rifted margins, *J. Geol. Soc. London* 161**,** 783-798.

Roger, J., Platel, J.P., Cavelier, C. & Bourdillon-de-Grisac, C., 1989. Données nouvelles sur la stratigraphie et l'histoire géologique du Dhofar (Sultanat d'Oman), *Bull. Soc. Geol. Fr.,* 2**,** 265-277.

Sage, F., Collot, J.Y. & Ranero, C.R., 2006. Interplate patchiness and subduction-erosion mechanisms: Evidence from depth-migrated seismic images at the central Ecuador convergent margin, *Geology,* 34**,** 997-1000.

Schroeder, T. & John, E.B., 2004. Strain localization on an oceanic detachment fault system, Atlantis Massif, 30°N, Mid-Atlantic Ridge, *Geochem. Geophys. Geosyst.,* 5**,** doi:10.1029/2004GC000728.

Shillington, D.J., Holbrook, W.S., Van Avendonk, H.J.A., Tucholke, B.E., Hopper, J.R., Louden, K.E., Larsen, H.C. & Nunes, G.T., 2006. Evidence for asymmetric nonvolcanic rifting and slow incipient oceanic accretion from seismic reflection data on the Newfoundland margin, *J. Geophys. Res.,* 111**,** doi:10.1029/2005JB003981.

Tamsett, D. & Searle, R., 1990. Structure of the Alula-Faartak fracture zone, Gulf of Aden, *J. Geophys. Res.,* 95**,** 1239-1254.

Tard, F., Masse, P., Walgenwitz, F. & Gruneisen, P., 1991. The volcanic passive margin in the vicinity of Aden, Yemen, *Bull. Cent. Rech. Explor. Prod. Elf-Aquitaine,* 15**,** 1-9.

Thierry, P., Lambaré, G., Podvin, P. & Noble, M., 1999. 3D preserved amplitude prestack depth migration on a workstation, *Geophysics,* 64**,** 222-229.

Tiberi, C., Leroy, S., d Acremont, E., Bellahsen, N., Ebinger, C., Al Lazki, A. & Pointu, A., 2007. Crustal geometry of the northeastern Gulf of Aden passive margin; localization of the deformation inferred from receiver function analysis, *Geophys. J. Int.,* 168**,** 1247-1260.

Tucholke, B.E., Sawyer, D.S. & Sibuet, J.C., 2007. Breakup of the Newfoundland Iberia rift, *Geol. Soc. Spec. Publ.,* 282**,** 9-46.

Vendeville, B., Cobbold, P.R., Davy, P., Choukroune, P. & Brun, J.P., 1987. Physical models of extensional tectonics at various scales, *Geol. Soc. Spec. Publ.,* 28**,** 95-107.

Vigny, C., Huchon, P., Ruegg, J.C., Khanbari, K. & Asfaw, L.M., 2006. Confirmation of Arabia slow plate motion by new GPS data in Yemen, *J. Geophys. Res.,* 111**,** doi:10.1029/2004JB003229.

Watchorn, F., Nichols, G.J. & Bosence, D.W.J., 1998. Rift-related sedimentation and stratigraphy, southern Yemen (Gulf of Aden). *in Sedimentation and tectonics in rift basins: Red Sea–Gulf of Aden*, pp. 165- 189, eds. Purser, B. H. & Bosence, D. W. J. Chapman & Hall, London.

Watremez, L., Leroy, S., Rouzo, S., d'Acremont, E. & Lucazeau, F., 2009. Crustal structure of the NE Gulf of Aden continental margin from wide-angle seismic data, *Geophys. Res. Abs., EGU General Assembly 2009,* Vol. 11, EGU2009-5527.

Weinberg, R.F., Regenauer-Lieb, K. & Rosenbaum, G., 2007. Mantle detachment faults and the breakup of cold continental lithosphere, *Geology,* 35**,** 1035–1038.

Wernicke, B.P., 1985. Uniform-sense normal simple shear of the continental lithosphere, *Can. J. Earth Sci.,* 22**,** 108-125.

White, R.S., McKenzie, D. & O'Nions, R.K., 1992. Oceanic crustal thickness from seismic measurements and rare earth element inversions, *J. Geophys. Res.,* 97**,** 19683–19715.

Whitmarsh, R.B., Manatschal, G. & Minshull, T.A., 2001. Evolution of magma-poor continental margins from rifting to seafloor spreading, *Nature,* 413**,** 150-154.

Whitmarsh, R.B. & Sawyer, D.S., 1996. The ocean/continent transition beneath the Iberia Abyssal Plain and continental-rifting to seafloor-spreading processes. *in Proc. ODP, Sci. Results*, pp. 713-733, eds. Whitmarsh, R. B., Sawyer, D. S., Klaus, A. & Masson, D. G.

Wilson, P.G., Turner, J.P. & Westbrook, G.K., 2003. Structural architecture of the ocean-continent boundary at an oblique transform margin through deep-imaging seismic interpretation and gravity modelling: Equatorial Guinea, West Africa, *Tectonophysics,* 374**,** 19-40.

Worzel, J.L., 1968. Advances in marine geophysical research of continental margins., *Can. J. Earth Sci.,* 5**,** 963–983.

Zelt, C., Sain, K., Naumenko, J.V. & Sawyer, D.S., 2003. Assessment of crustal velocity models using seismic refraction and reflection tomography, *Geophys. J. Int.*, 153, 609-626.

Figure 1. Bathymetric and topographic map of the Gulf of Aden area and divergence directions. Small pink circles represent seismicity (Mw > 5 1964-2007) (IRIS, http://www.iris.edu). AFFZ: Alula-Fartak fracture zone; SHFZ: Socotra-Hadbeen fracture zone; SR: Sheba Ridge; OFZ: Owen faults zone; SESFZ: Shukra El Sheik fracture zone. The red square indicates the study area on the northern margin of the Gulf of Aden.

Figure 2. Track map of the Encens cruise (Leroy *et al.* 2006; Leroy *et al.* submitted). The first-order segment between the Alula-Fartak fracture zone (AFFZ) and the Socotra-Hadbeen fracture zone (SHFZ) is divided into three second-order segments: Ashawq-Salalah, Taqah and Mirbat segments. The ES08 profile is taken from the Encens-Sheba cruise data (Leroy *et al.* 2004). Onshore geological map from Bellahsen *et al.* (2006) and references therein.

Figure 3. Seismic facies and different units proposed for the stratigraphy of the profiles, as defined in the distal part of the offshore margin on the MCS profile ENC34, and sedimentary formations of the proximal part of the margin cropping out onland. The onshore stratigraphy and subsidence history is from Platel & Roger (1989), Roger *et al.* (1989), Platel *et al.* (1992) and Leroy *et al.* (2007). We propose a correlation of the onshore/offshore series based on the following hypothesis: offshore sedimentation may be poorly developed (thin deposits) when onshore sedimentation is thick (and *vice versa*). See text for explanation.

Figure 4. Top: Pre Stack Depth Migration (PSDM) section of ENC34 line, with no vertical exaggeration. The position of the 5d anomaly indicated by a solid line is from Leroy *et al.* (2004), corresponding to the boundary between the reversed and normal block of the old 5d anomaly. Bottom: examples of Iso-X panels (traces sorted by common-angle gathers for a given x-coordinate) used for the PSDM. The main reflectors are identified.

Figure 5. (a) Shaded-relief bathymetric map of the Encens-Sheba (Leroy *et al.* 2004) and Encens cruises (Leroy *et al.* 2006). (b) Depth to acoustic basement map of the study area constructed using all the Encens cruise profiles located in the study area. (c). Offshore structural pattern (this study) and onshore geological map from Bellahsen *et al.* (2006 and references therein). Thin black lines indicate the ship's track, and thick black lines

indicate the seismic lines shown in this study.

Figure 6. Seismic lines (top) and line drawings (bottom) of seismic lines ENC32, ENC34 and ENC35. The location of the three crustal domains is that proposed by d'Acremont *et al.* (2005), modified in this study for the northern boundary of the OCT. The position of the 5d anomaly indicated by an arrow is taken from Leroy *et al.* (2004), corresponding to the boundary between the reversed and normal block of the old 5d anomaly. The sedimentary units are labelled as syn-rift (U1), syn-OCT (U2) and post-rift (U3, U4 and U5). The thick line represents the acoustic basement. The arrows indicate the location of the main basement highs of the distal margin on each profile. (a) Location of the three profiles. (b) Sketch of syn-rift wedges re-faulted during the final syn-rift stage in the 'DIM graben' area.

Figure 6. (*Continued.*)

Figure 7. Interpretation of the sedimentary sequence of the DIM graben on the ES08 line, equivalent to the ENC32 line. Note geometry of strata around the OCT ridge indicating growth of this feature. Inset: location of the ES08 profile.

Figure 8. ENC34 pre-stack depth migrated section and interpretation. Key sites are indicated in detail and localized on the full PSDM profile (at the top), identified by letters (a, b, c and d). Each key site is presented without (top) and with its interpretation (bottom). (c) The DIM graben is interpreted in the left panel on the vertically exaggerated time section, to allow a better comparison of the seismic patterns.

Figure 8. (*Continued.*)

Figure 9. Structural evolution of the Ashawq-Salalah segment based on interpretation of the pre-stack depth migration of the ENC34 profile. (a) Syn-rift stage: Large offset normal faults may root on the brittle–ductile transition (BDT), tilting the pre-rift sediments and delimiting syn-rift grabens (perched and DIM). (b) Late syn-

rift stage: Localization of extension: the continuous thinning of the brittle crust leads to the formation of less widely spaced faults. (c) OCT stage: differential vertical movements between proximal and distal parts of the margin result in a submarine landslide on the southernmost tilted block. The OCT may be formed by exhumation of the underlying partly serpentinized mantle in the break-up zone. The flat syn-OCT unit emplaced in the DIM and perched grabens predates the spreading initiation of spreading. (d) Initiation of spreading: The continental break-up takes place when mantle finally reaches the surface, which then localizes the emplacement of the spreading. (e) Post-rift stage: The ENC34 volcano is progressively built up by several volcanic events and resulting uplifts. The boundary between serpentinised mantle and ductile crust (question mark) is difficult to define under the DIM graben.

Figure 10. Timing and evolution of the OCT ridge from spreading time to present, based on interpretation of the ES08 profile presented in Figure 7. (a) Onset of post-rift stage: a slight uplift is marked by an erosional surface and slight tilting of the OCT ridge toward the north. (b) Early post-rift stage: a general transgression associated with the deposition of U3L. (c) Middle post-rift stage: major growth of the basement high (OCT ridge) during deposition of U3U. (d) Late post-rift stage: slight vertical movements of the OCT ridge may be coeval with the infilling. (e) Present day: recent seafloor deformation may eventually occur.
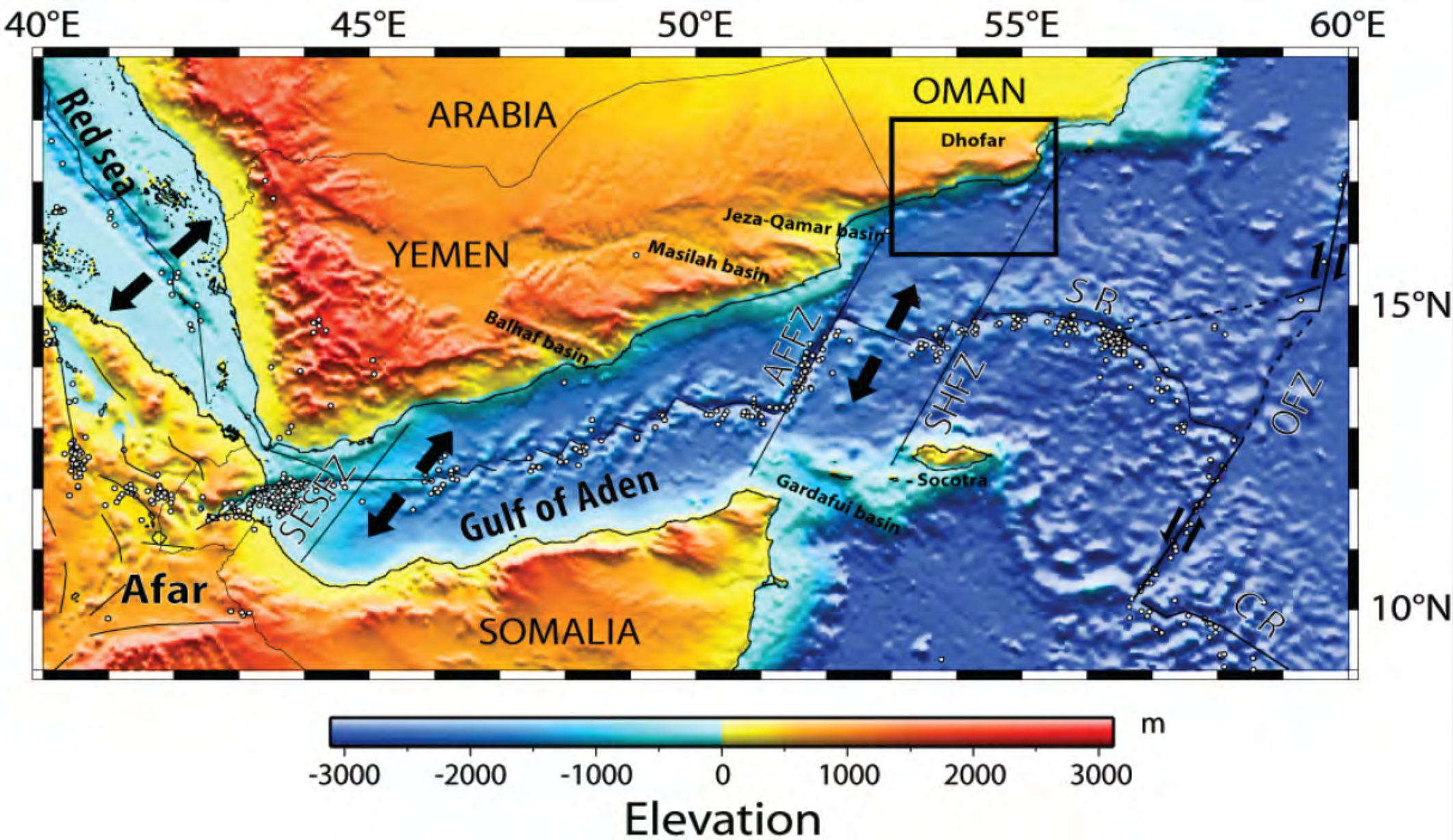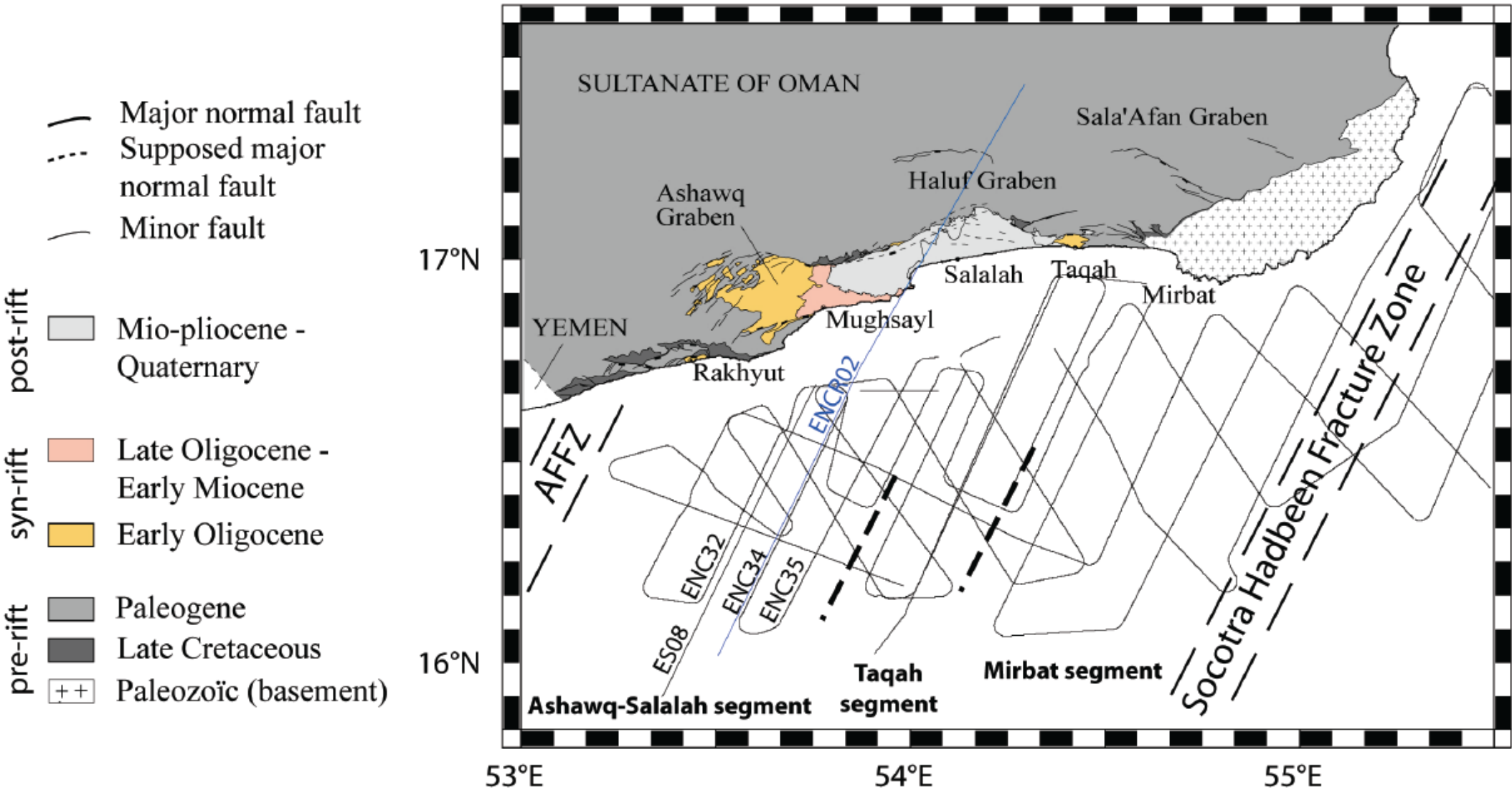
OFFSHORE ← → | ← → ONSHORE
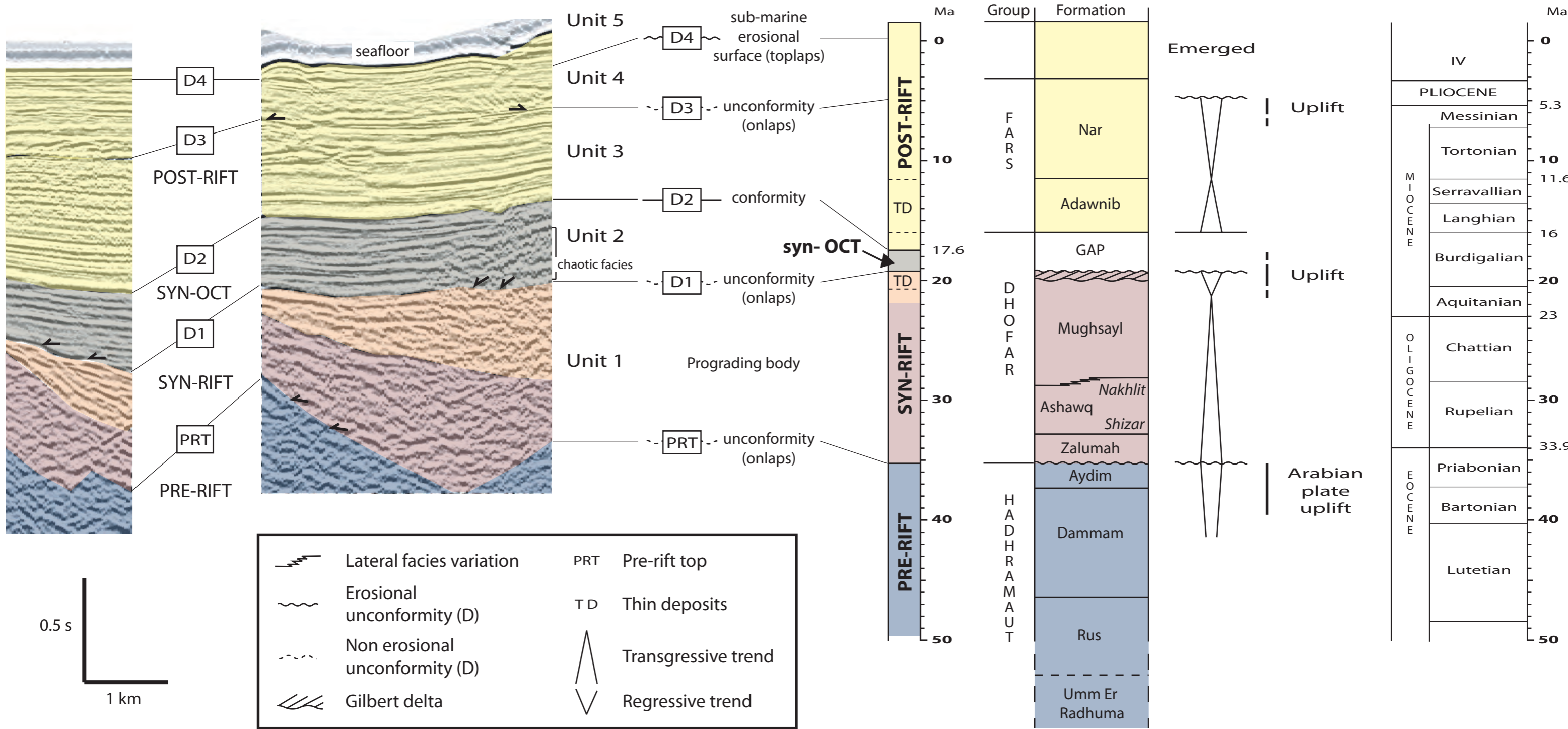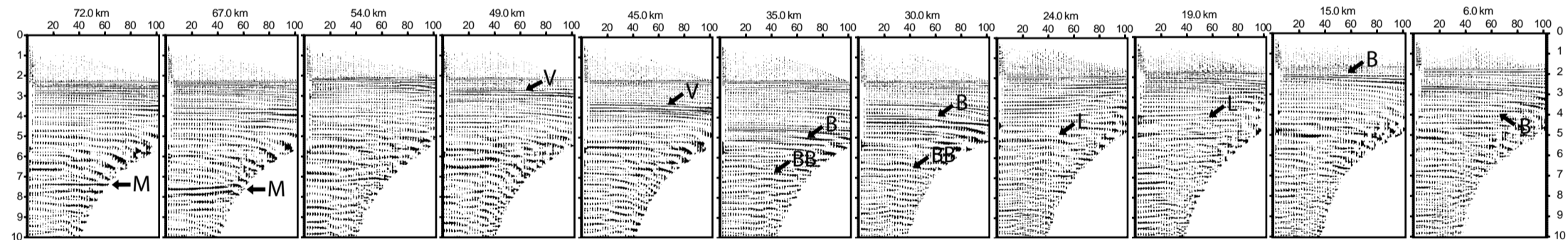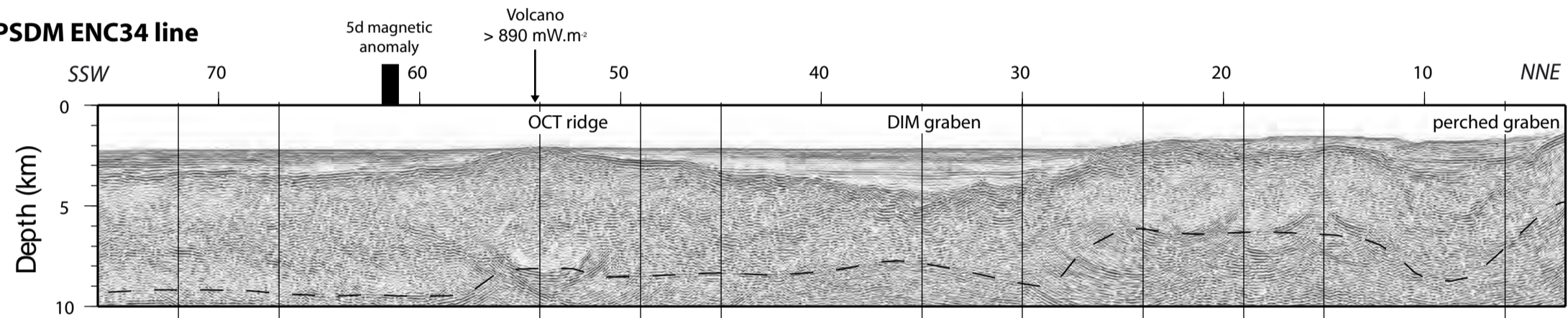
DIM graben

Perched graben

Boundaries

Onshore units

Subsidence evolution in the Dhofar area

Unit 5
D4 — sub-marine erosional surface (toplaps)
seafloor

Unit 4
D3 — unconformity (onlaps)

POST-RIFT

Unit 3

D2 — conformity

Unit 2
chaotic facies

syn- OCT

D1 — unconformity (onlaps)

Unit 1
Prograding body

PRT — unconformity (onlaps)

D4
D3
POST-RIFT
D2
SYN-OCT
D1
SYN-RIFT
PRT
PRE-RIFT

Ma
0

POST-RIFT

10

TD

17.6
20

TD

SYN-RIFT

30

PRE-RIFT

40

50

Group | Formation

FARS | Nar
| Adawnib

GAP

DHOFAR | Mughsayl
| Nakhlit
Ashawq | Shizar
| Zalumah

HADHRAMAUT | Aydim
| Dammam
| Rus
| Umm Er Radhuma

Emerged

Uplift

Uplift

Arabian plate uplift

Ma
0

IV

PLIOCENE
5.3
Messinian

Tortonian
10
11.6
MIOCENE | Serravallian

Langhian
16
Burdigalian

20
Aquitanian
23

OLIGOCENE | Chattian

Rupelian
30
33.9

EOCENE | Priabonian

Bartonian
40

Lutetian

50

0.5 s

1 km

⌁ Lateral facies variation
∿ Erosional unconformity (D)
- - - Non erosional unconformity (D)
⫸ Gilbert delta

PRT Pre-rift top
T D Thin deposits
◇ Transgressive trend
∨ Regressive trend

PSDM ENC34 line

Volcano
> 890 mW.m⁻²

SSW   70   60   50   40   30   20   10   *NNE*

OCT ridge   DIM graben   perched graben

Depth (km)

0

5

10

72.0 km   67.0 km   54.0 km   49.0 km   45.0 km   35.0 km   30.0 km   24.0 km   19.0 km   15.0 km   6.0 km

20 40 60 80 100   20 40 60 80 100   20 40 60 80 100   20 40 60 80 100   40 60 80 100   40 60 80 100   40 60 80 100   20 40 60 80 100   20 40 60 80 100   20 40 60 80 100   20 40 60 80 100

V   V   B   B   B

M   M   BB   BB   L

IsoX panels

— — multiple of the top of the acoustic basement   B   Basement   no vertical exaggeration

M   Moho   BB   Brittle deformation base

V   Volcanics   L   Landslide
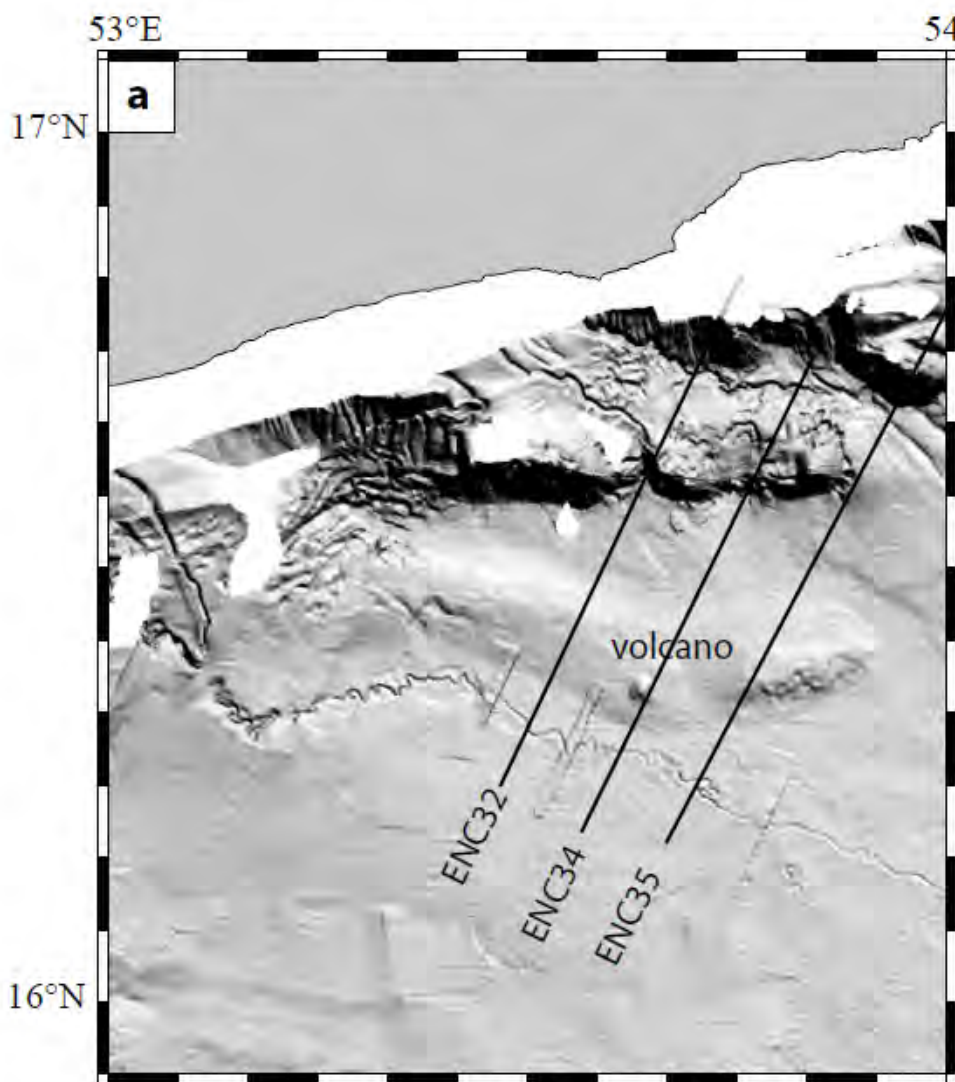
Shaded-relief bathymetric map

Depth to acoustic basement

m

-6000   -4000   -2000   0
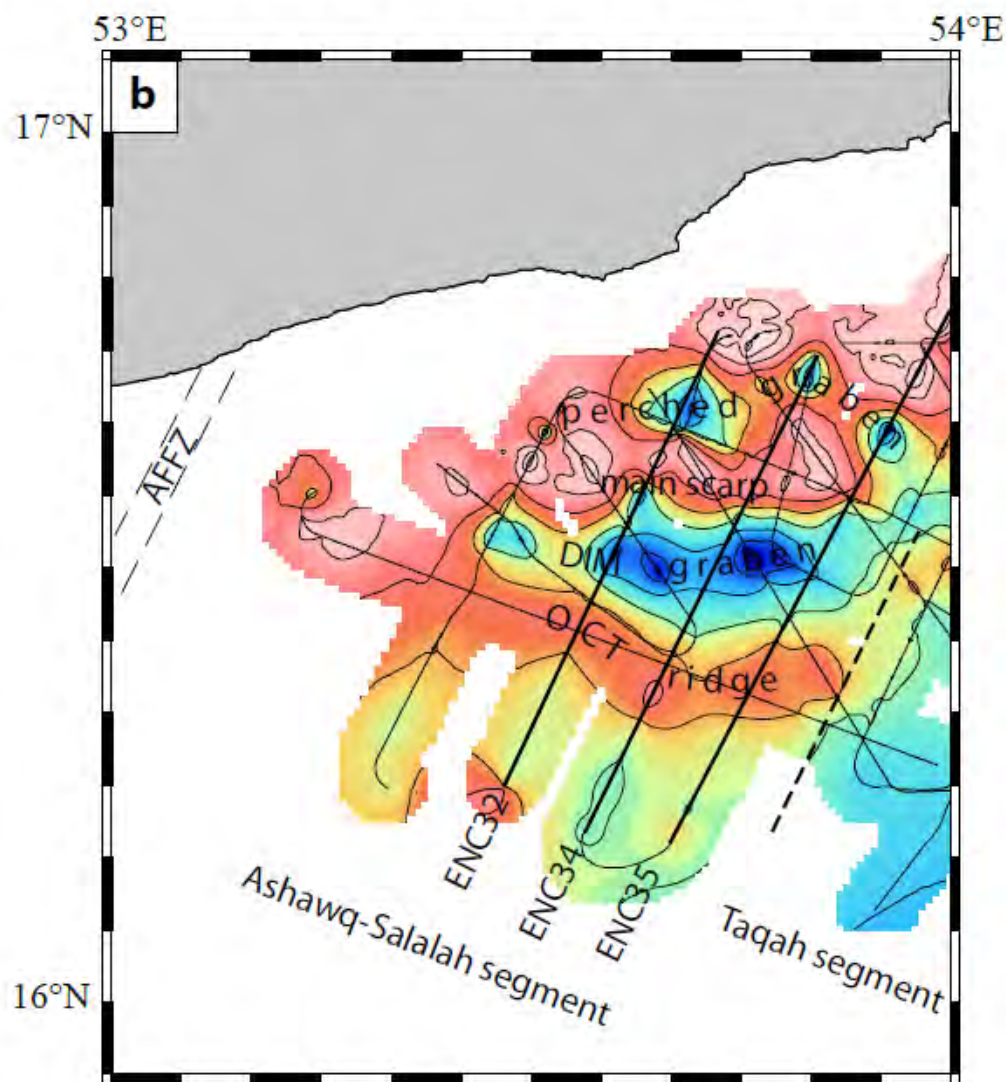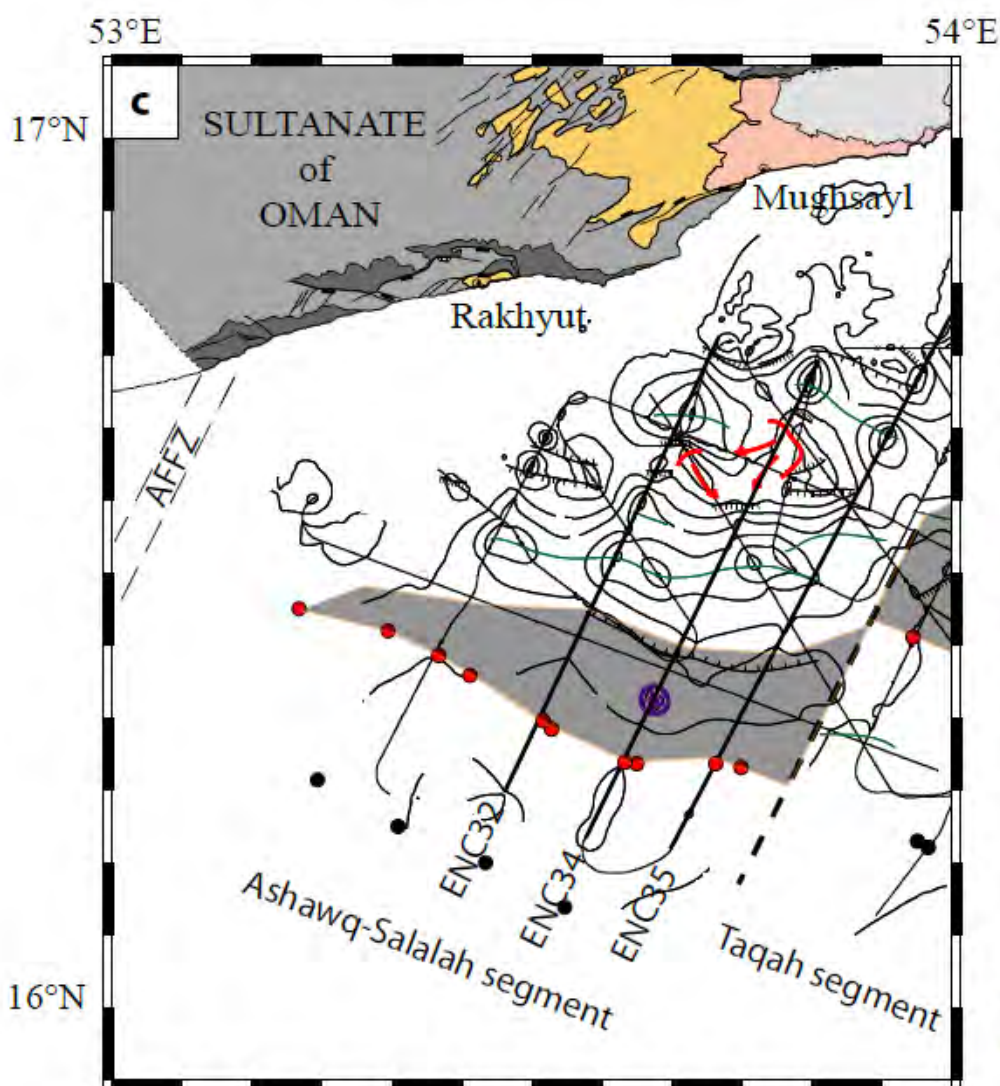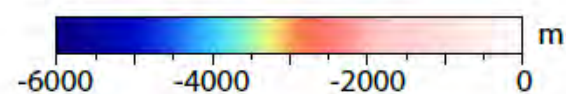
Onshore:

— Major normal fault

···· Supposed major normal fault

— Minor fault

post-rift

Mio-pliocene - Quaternary

syn-rift

Late Oligocene - Early Miocene

Early Oligocene

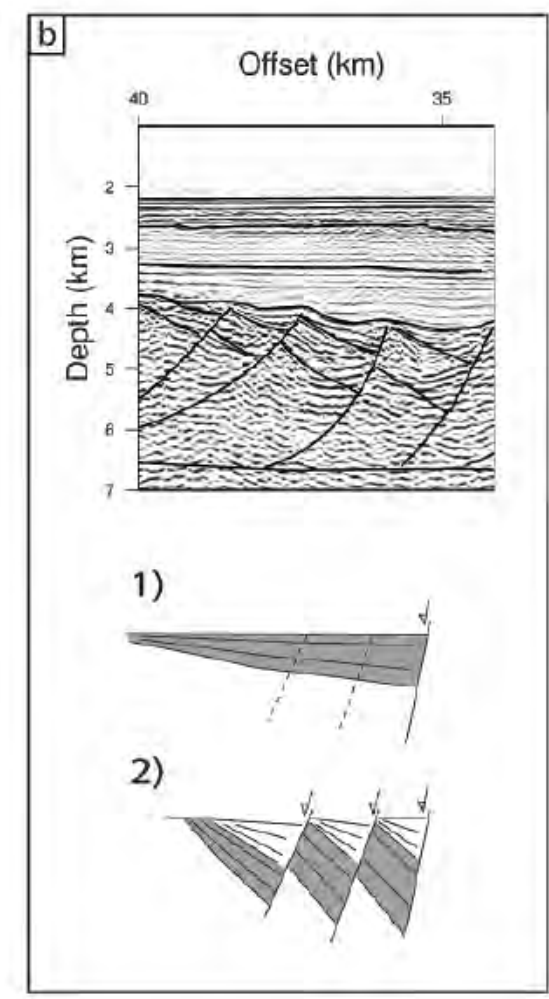pre-rift

Paleogene

Late Cretaceous

⊞ Paleozoïc (basement)

Offshore:

Ocean-Continent Transition

Normal fault

Maximal basin depth line

Sliding direction on the landslide

● 5d magnetic anomaly

● 5c magnetic anomaly

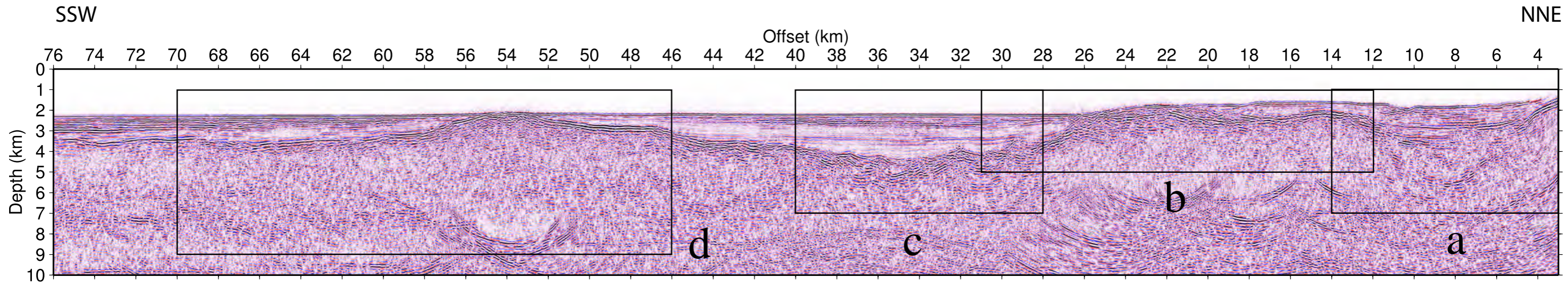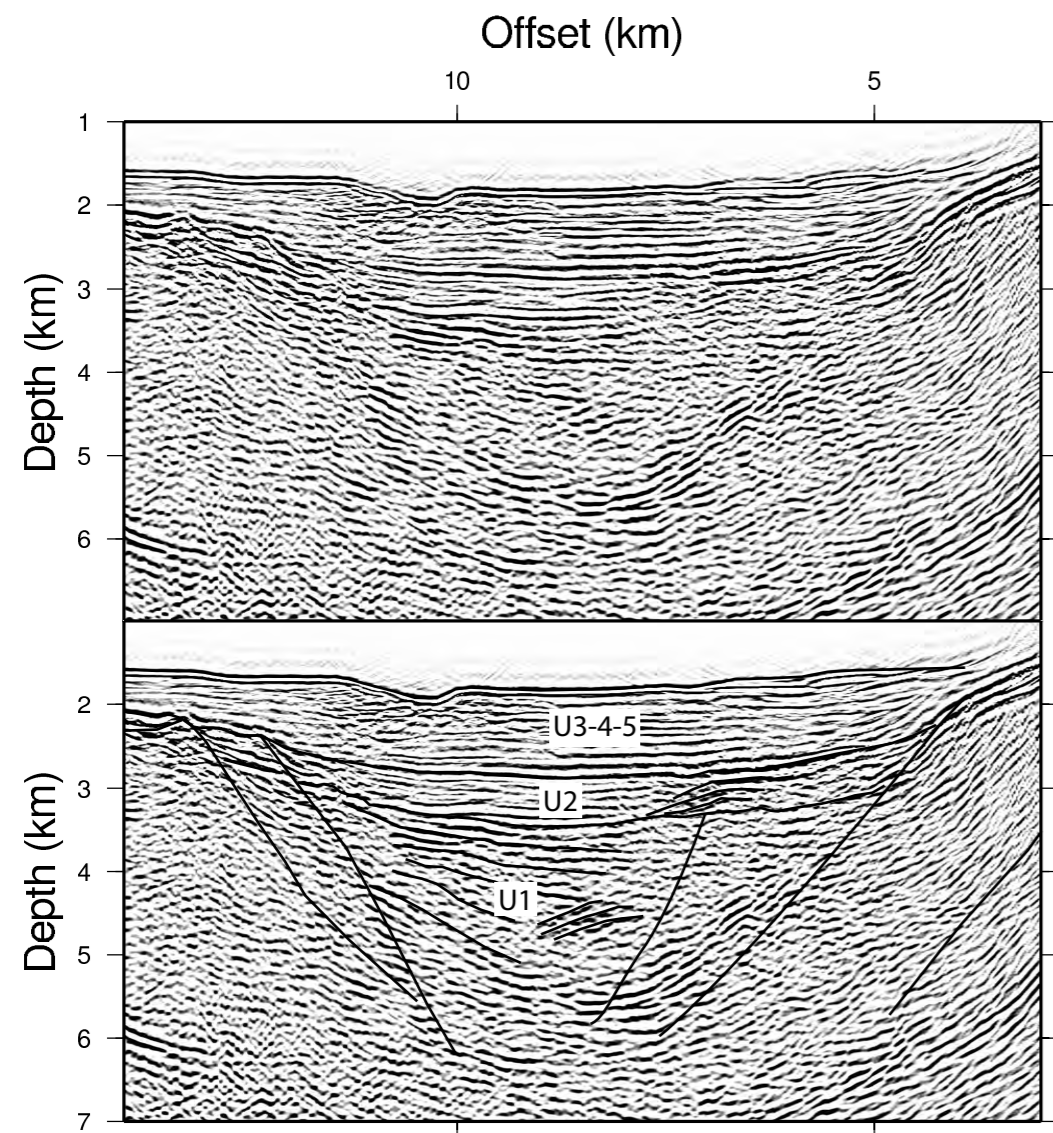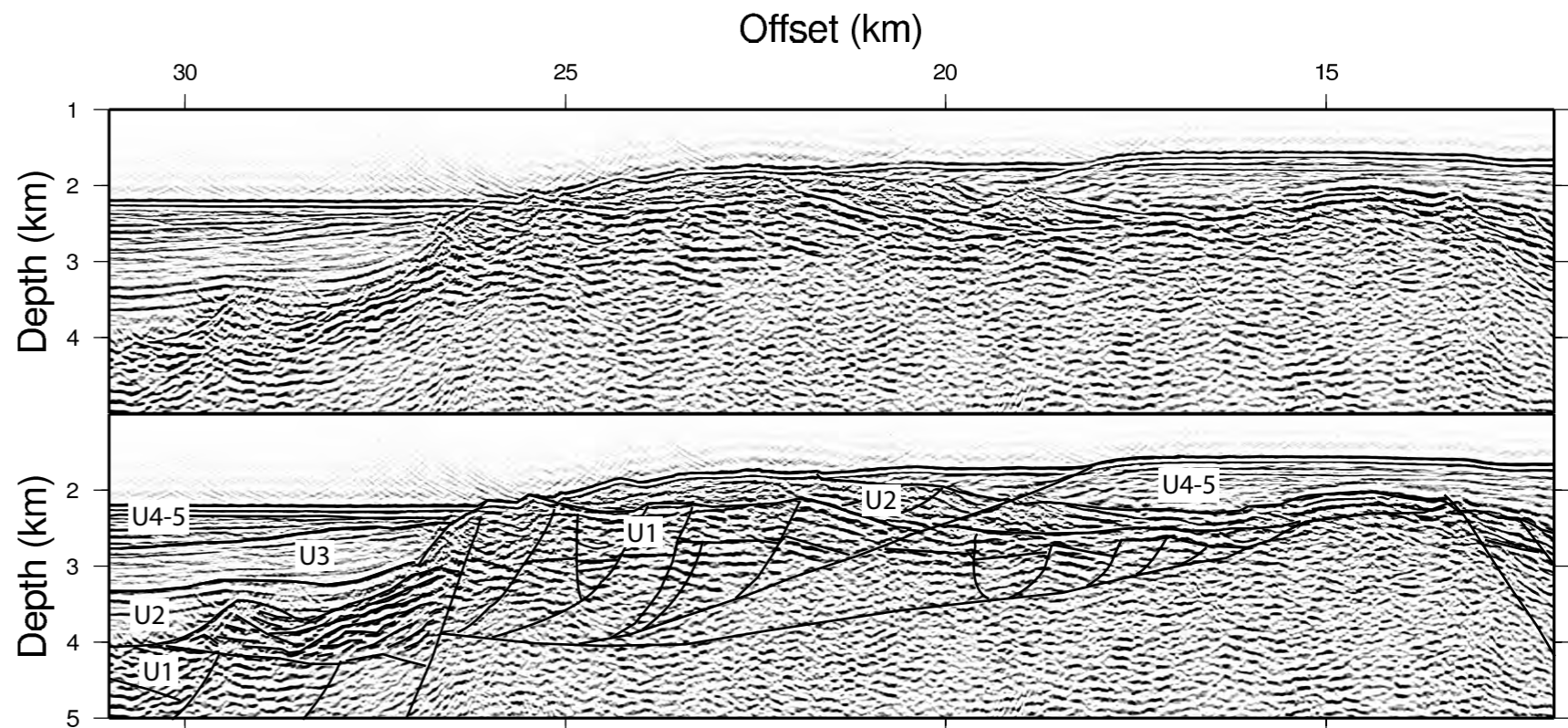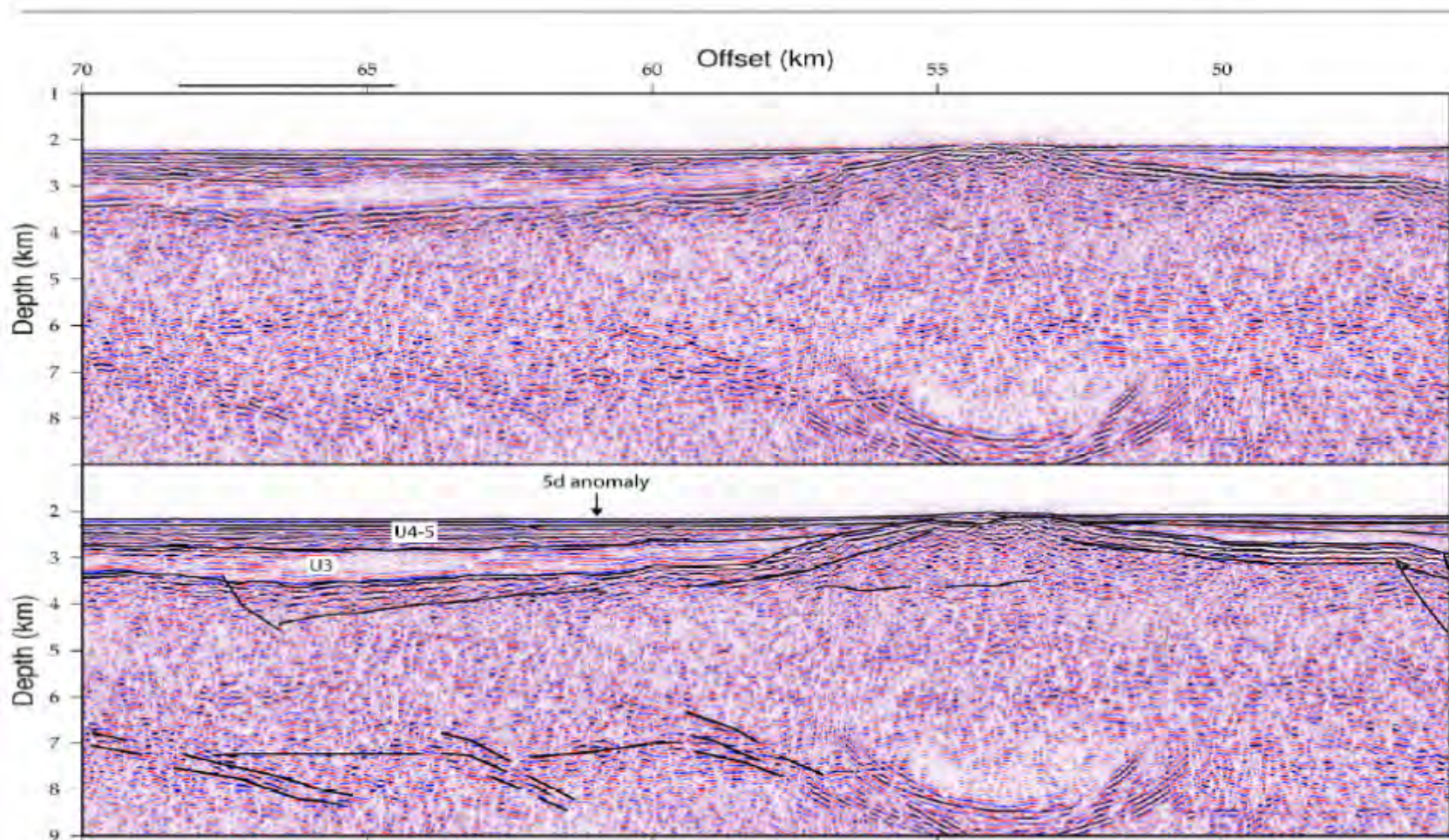**Structural scheme on the acoustic basement isodepth lines.**

SSW ... *NNE*

OCT ridge — DIM graben — Perched graben

5d magnetic anomaly

Depocenter

ENC32 — OCEANIC CRUST — OCEAN–CONTINENT TRANSITION — CONTINENTAL CRUST

CDP number

ENC34 — OCEANIC CRUST — OCEAN-CONTINENT TRANSITION — CONTINENTAL CRUST

CDP number

ENC35 — OCEANIC CRUST — OCEAN-CONTINENT TRANSITION — CONTINENTAL CRUST

CDP number

Vertical exaggeration in the sedimentary cover: × 1.24

a — OMAN — AFFZ — ENC30 — ENC32 — ENC34 — ENC35 — Ashawq-Salalah segment — Taqah segment

SSW
OCT ridge DIM graben Perched graben NNE

5d magnetic anomaly

ENC32 OCEANIC CRUST OCEAN-CONTINENT TRANSITION CONTINENTAL CRUST

ENC34 OCEANIC CRUST OCEAN-CONTINENT TRANSITION CONTINENTAL CRUST

ENC35 OCEANIC CRUST OCEAN-CONTINENT TRANSITION CONTINENTAL CRUST

Vertical exaggeration in the sedimentary cover: × 1.24

SSW   NNE

Unit boundaries
Acoustic Basement top
Erosional surface
Toplap / Onlap

5 km

Vertical exaggeration : x 10.4

DIM graben

Unit 5

Unit 4

Unit 3U

OCT ridge

Unit 3L

U1

acoustic basement

acoustic basement

Unit 2

Unit 1

ES08

TWTT (ms)

CDP number

SSW / NNE seismic section with Offset (km) along top and Depth (km) along left axis. Labeled boxes: d, c, b, a.

a : Perched graben

Labels: U3-4-5, U2, U1

b : Landslide

Labels: U4-5, U3, U2, U1

c : DIM graben

CDP number

TWTT (ms)

Offset (km)

Depth (km)

U4-5
U3
U2
U1

Time section with vertical exaggeration : X 2

No vertical exaggeration

Offset (km)

Depth (km)

5d anomaly

U4-5
U3

d : Volcano

> 890 mW.m^{-2}
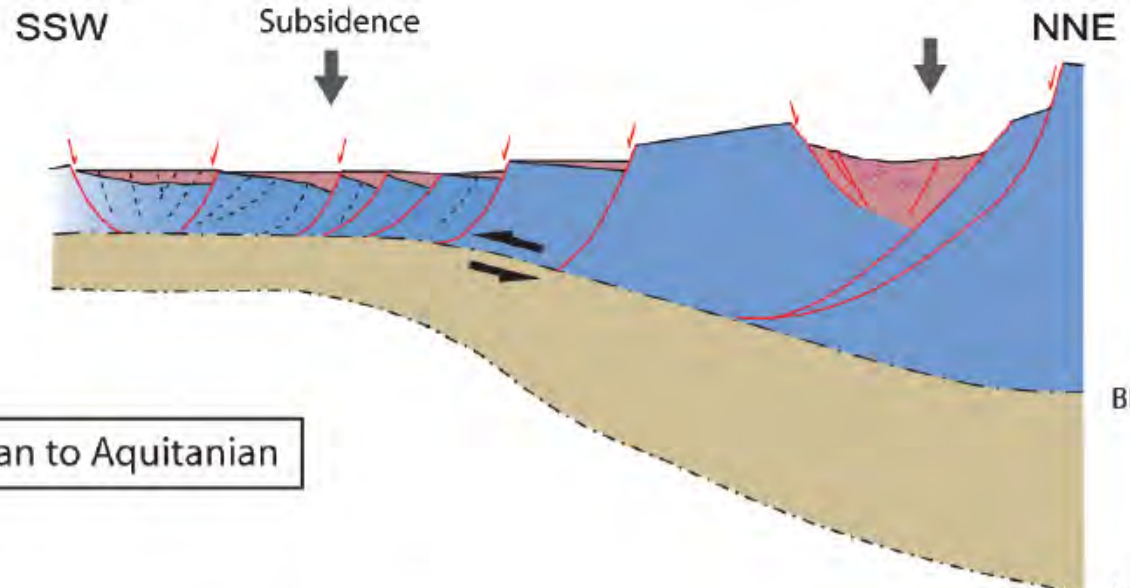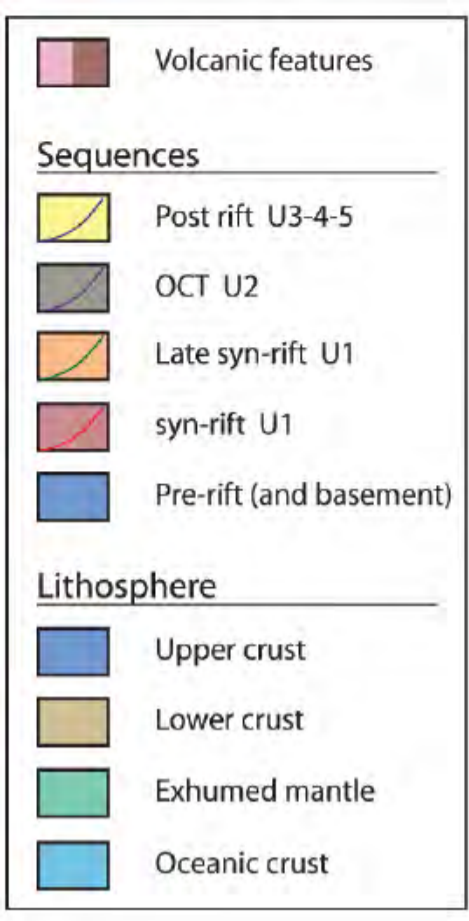
ENC34

Profile location (black line) and morphology of the volcano on the multi-beam bathymetry.

Volcanic features

Sequences
- Post rift U3-4-5
- OCT U2
- Late syn-rift U1
- syn-rift U1
- Pre-rift (and basement)

Lithosphere
- Upper crust
- Lower crust
- Exhumed mantle
- Oceanic crust

5 km
5 km

SSW   Subsidence   NNE

syn-rift time
a) 35-21 Ma: Priabonian to Aquitanian

BDT

Moh

Subsidence

late syn-rift time
b) ~21-19 Ma: late Aquitanian-early Burdigalian

Landslide

Uplift
onland

OCT time
c) ~19-18 Ma: middle Burdigalian

?

Proto-Sheba ridge

spreading initiation
d) 17.6 Ma: late Burdigalian

Asthenosphere

?

SSW   5d magnetic anomaly   volcano   NNE

Depth (Km)

8 km
?

post-rift time (see figure 10)
e) 17.6 Ma to present: final Burdigalian to present

— · — · — Mid crustal boundary constrained by wide-angle seismic
— · — · — Moho reflection constrained by wide-angle seismic

SSW   NNE

Time

a) Onset of post-rift time

OCT ridge   OCT graben

Erosional surface

?

Small volcano-sedimentary wedge
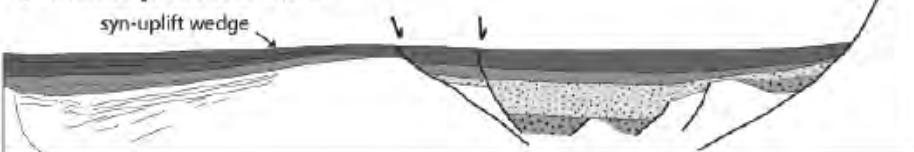
SYN-RIFT PRE-STRUCTURATION
SYN-OCT TIME FILLING
SLIGHT UPLIFT
LOCAL OR GENERAL EROSION

b) Early post-rift time

TRANSGRESSION
NO OCT RIDGE GROWTH

c) Middle post-rift time

syn-uplift wedge

MAJOR UPLIFT OF
THE OCT RIDGE

d) Late post-rift time

FILLING WITH SLIGHT
RIDGE GROWTH

e) Present time

slight deformation of the seafloor
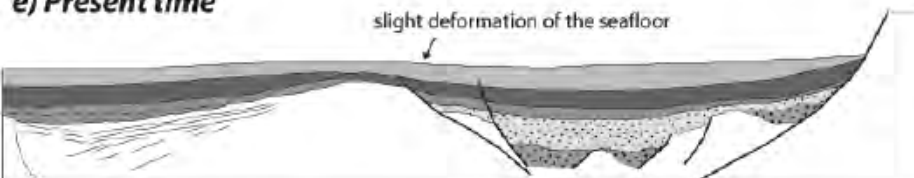
POSSIBLE RECENT
SEAFLOOR DEFORMATION

Unit 4-5

Upper Unit 3 } Post-rift time

Lower Unit 3

Unit 2 - OCT time

Unit 1 - syn-rift time

Acoustic basement

Faults initiated during syn-rift time

Vertical exaggeration : × 3

1 km

5 km